Archimedes Optimizer: Theory, Analysis, Improvements, and Applications

Krishna Gopal Dhal[1] · Swarnajit Ray[2] · Rebika Rai[3] · Arunita Das[1]

Abstract

The intricacy of the real-world numerical optimization tribulations has full-fledged and diversely amplified necessitating proficient yet ingenious optimization algorithms. In the domain wherein the classical approaches fall short, the predicament resolving nature-inspired optimization algorithms (NIOA) tend to hit upon an excellent solution to unbendable optimization problems consuming sensible computation time. Nevertheless, in the last few years approaches anchored in nonlinear physics have been anticipated, announced, and flourished. The process based on non-linear physics modeled in the form of optimization algorithms and as a subset of NIOA, in countless cases, has successfully surpassed the existing optimization methods with their effectual exploration knack thus formulating utterly fresh search practices. Archimedes Optimization Algorithm (AOA) is one of the recent and most promising physics optimization algorithms that use meta-heuristics phenomenon to solve real-world problems by either maximizing or minimizing a variety of measurable variables such as performance, profit, and quality. In this paper, Archimedes Optimization Algorithm (AOA) has been discussed in great detail, and also its performance was examined for Multi-Level Thresholding (MLT) based image segmentation domain by considering t-entropy and Tsallis entropy as objective functions. The experimental results showed that among recent Physics Inspired Optimization Algorithms (PIOA), the Archimedes Optimization Algorithm (AOA) produces very promising outcomes with Tsallis entropy rather than with t-entropy in both color standard images and medical pathology images.

Keywords Nature-inspired optimization algorithms · Image segmentation · Optimization · Tsallis · t-entropy · Archimedes optimization algorithm · Physics inspired optimization algorithms

1 Introduction

As the name suggests, meta-heuristics in computer science and mathematics are high-level processes or heuristic designs used to create algorithms that can nevertheless offer an adequate solution to an optimization issue, despite the limited processing capability. Most of the time use of conventional methods to optimize some problem takes a long time. Therefore compromising somewhat on the quality of the solution, which may not find the optimal solution, but we will find a solution that is sufficient for our needs, and we can do this very efficiently with a meta-heuristic algorithm. Among the various meta-heuristic algorithm some are inspired by our nature or mimic some behavior from our nature. Commonly, nature-inspired algorithms are employed to solve a variety of optimization challenges. There have been several meta-heuristics developed in the last three decades to help solve complicated and real-world problems in a variety of sectors. These meta-heuristics algorithms draw

✉ Swarnajit Ray
 swarnajit32@gmail.com

 Krishna Gopal Dhal
 krishnagopal.dhal@midnaporecollege.ac.in

 Rebika Rai
 rrai@cus.ac.in

 Arunita Das
 arunita.das@midnaporecollege.ac.in

[1] Department of Computer Science and Application, Midnapore College (Autonomous), Paschim Medinipur, Midnapore, West Bengal, India

[2] Department of Computer Science and Engineering, Maulana Abul Kalam Azad University of Technology, Kolkata, West Bengal, India

[3] Department of Computer Applications, Sikkim University, Gangtok, Sikkim, India

a huge amount of attention to researchers and scientists due to their complex problem-solving capability. Meta-heuristics algorithms can be used in many different fields, such as computer science, image processing, control systems, electrical engineering, different types of classification, etc. According to the No Free Lunch Theorem, "all optimization algorithms perform equally well when their performance is averaged across all possible problems". That means one can't say that one optimization is good for solving all types of optimization task. It is application dependent. So, the researcher tries to invent a new algorithm or improve the existing one according to their requirements. New NIOAs are always a good thing for the research field, as long as they solve problems quickly and effectively. One can classify these optimization problems according to the solution originated or the behavior of the algorithms. Figure 1 shows the classification of meta-heuristic algorithms.

Image segmentation is the branch of digital image processing which primarily emphasizes on sectionalization of an image into numerous shares as per their features or properties basically for easier analysis of imagery. Various methods of segmentation are extensively employed [1, 2] namely thresholding-based, boundary-based, region-based,

clustering-based [3, 4], and hybrid technique based, and amongst all the methods, thresholding-based is the most popular one. Multi-Level Thresholding (MLT) image segmentation has attained significant attention in quite a lot of image processing applications [5]. Nevertheless, the usage of traditional thresholding methods in determining the optimal threshold values (as a part of preprocessing step) is not just time-consuming but computationally demanding. This leads to the requirement of extension and attachment of certain procedures that might resolve the issue thus actuating the curiosity and interest in several academic scholars. Enormous research attempts are made during recent years toward solving real-world optimization problems with exceptionally towering dimensional search space, and rigorous constraints with nonlinear objective functions. More than a few mathematical elucidations rather than traditional optimization methods have been provided by a variety of researchers to work out the optimization problems however, the complexity of such mathematical solutions turned out to be very high requiring enormous computational time thereby proving to be ineffective in providing comprehensive solution in such circumstances. This pursuit consequently leads in the direction of the requirement for several modern technological
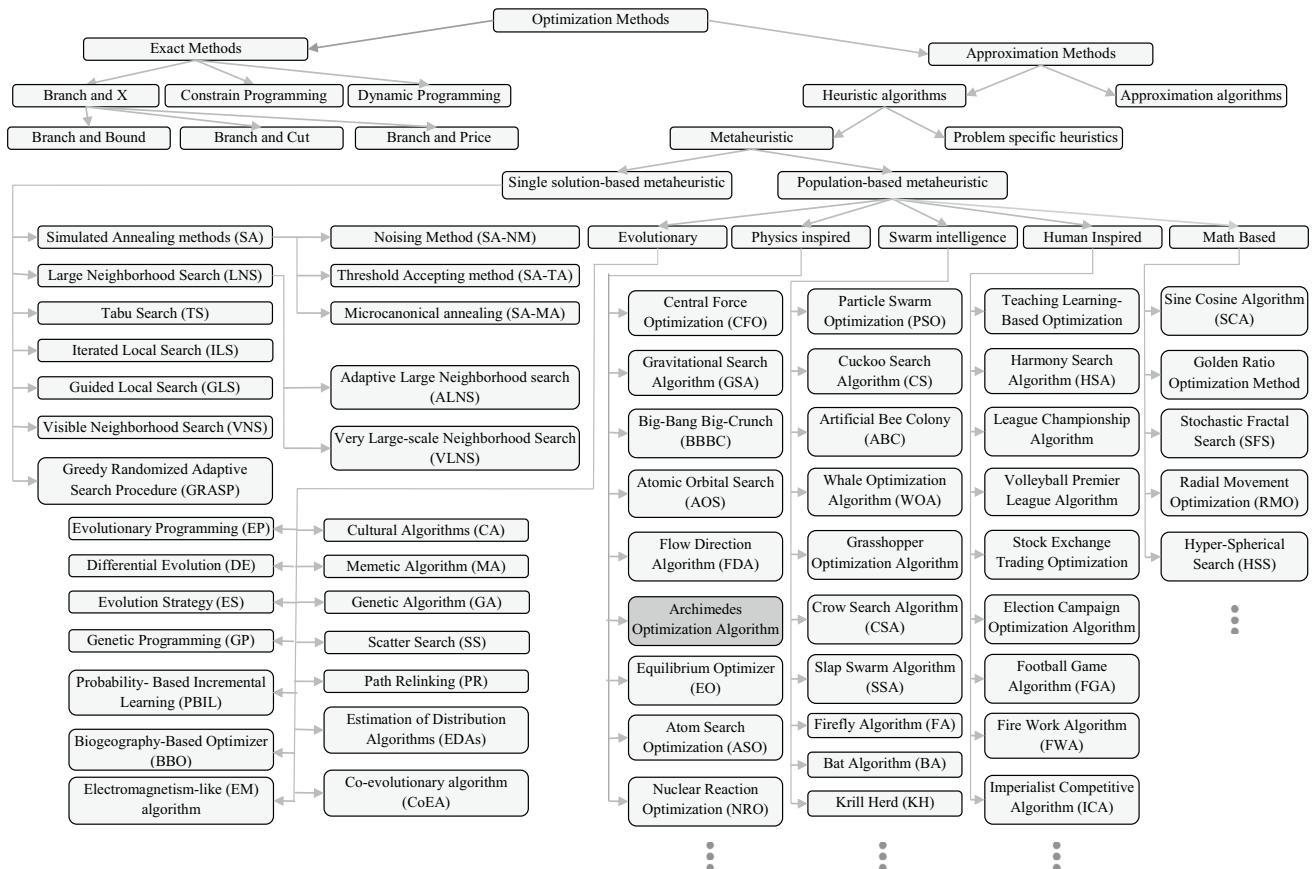

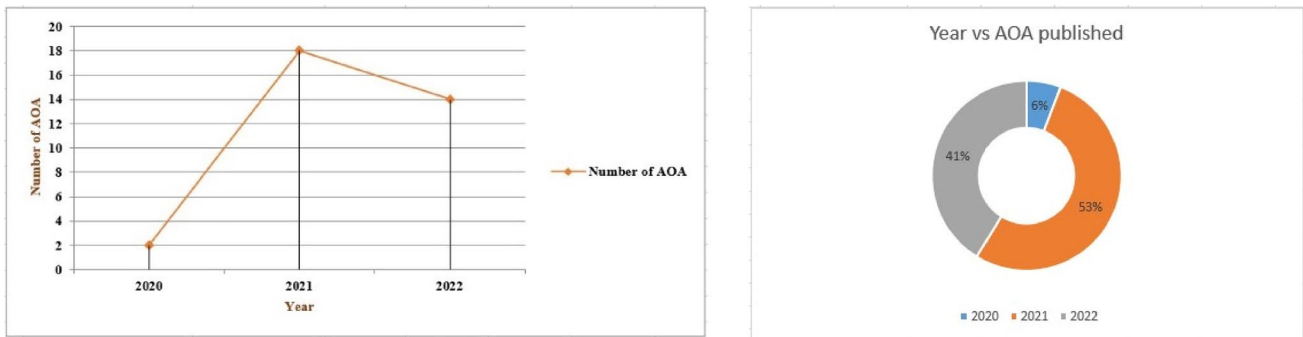**Fig. 1** Classification of optimization methods

Fig. 2 Year-wise AOA-based research work proposed

optimization processes that would be proficient enough to accomplish the most favorable general yet thriving solution bearing in mind time, complexity, and other checks.

In light of this, NIOA [6] and their upgraded variations and subset whose solutions were based on chemical, physical, and biological phenomena in nature showed their usefulness in engineering optimization issues and also in resolving a number of MLT problems [7]. These nature-inspired solutions happen to be incredibly trendy as they offered to a large extent improved solutions in terms of efficiency and complexity than earlier methods. However, in recent years methodologies associated with nonlinear physics have flourished; therefore, across a wide range of applications, nonlinear procedures-based algorithms are more effective and versatile than other approaches published previously. Numerous global optimization strategies more notably; unique searching strategies based on various nonlinear physics phenomena are a popular current trend in NIOA design leading to the introduction of the Physics Inspired Optimization Algorithm (PIOA). The uniqueness of this method is that nonlinear processes [8] may perhaps be used as a brainwave for building up flourishing search algorithms that principally tag along with the nonlinear directives originated in natural systems [9]. Such approaches appear to be more challenging to develop than other search methodologies, since they need not only the use of a novel, natural nonlinear method as the searching basis, but also modeling an effective adaption of that

procedure for addressing optimization issues. In order to build a completely new optimization algorithm following nonlinear processing modeling, this can be a challenging task and may require an expensive design method. In addition, this modeling may demand the tweaking of a set of algorithm parameters that are often connected with physical sub-processes inside the primary nonlinear process.

In this paper, a brief study has been performed on the Archimedes Optimization Algorithm (AOA) [10] which is a most recent and one of the most promising physics-inspired algorithm in the domain of optimization. This AOA is motivated by the physics phenomenon and here author evaluated, assessed, documented, and profoundly experimented with two types of images namely standard color images and pathology images by employing AOA. This paper mostly talks about AOA, its variations and improvements, and how Tsallis and t-entropy can be used to improve MLT image segmentation. Here, Tsallis and t-entropy are used as objective functions. Among all PIOA-based algorithms, AOA gives the best result in both Tsallis and t-entropy. But AOA with Tsallis entropy outperformed AOA with t-entropy in most of the cases with 4, 6, and 8 threshold values. Furthermore, we can conclude that AOA with Tsallis entropy gives superior results for medical pathology images rather than standard color images. Details discussion done in results section (Sect. 6) and conclusion section (Sect. 7). Several recently introduced Physics Inspired Optimization

Table 1 Recently introduced Physics-Inspired Optimization Algorithms (PIOA)

Sl	Name	Author	Year	Citation
1	Archimedes Optimization Algorithm (AOA) [10]	Hashim et al.	2021	214
2	Atomic Orbital Search (AOS) [11]	Azizi	2021	41
3	Flow Direction Algorithm (FDA) [12]	Karami et al.	2021	24
4	Equilibrium Optimizer (EO) [13]	Faramarzi et al.	2020	650
5	Henry Gas Solubility Optimization (HGSO) [14]	Hashim et al.	2019	359
6	Atom Search Optimization (ASO) [15]	Zhao et al.	2019	244
7	Nuclear Reaction Optimization (NRO) [16]	Wei et al.	2019	38

Algorithms (PIOA) have been included in Table 1 with Google Scholar Citation underlined (Dated: 17.07.2022).

In this paper, the author mainly concentrates on Archimedes Optimization Algorithm (AOA). The AOA is one of the most promising methods among the various PIOA-based optimization methods which is proposed in recent years (Fig. 2). This AOA-based method is widely used in the energy section, especially in the wind energy domain. The use of the AOA method in the image processing domain is surprisingly very low, though it performs very well in this domain. We have evaluated the performance of the AOA in the multi-level image segmentation domain in this paper in Sect. 6. Figure 4 represents the details analysis of the AOA method used in the different research fields. The author found most of the papers on AOA were published in different journals and only two papers were found which are published at the conference Fig. 3b.

Consequently, the following are the principal contributions of the paper:

- A very little effort was done before exploring AOA-based multi-level thresholding for image segmentation thereby this paper focuses on a brief study on AOA and the implementation and application of the seven recently developed PIOA in multi-level image segmentation domain.
- Only Differential Evolution (DE) has been used with t-entropy for Multi-Level Thresholding in the original finding paper of t-entropy [17]. This research work uses the Tsallis entropy and the newly constructed t-entropy as objective functions. As per the best of knowledge and research, t-entropy has not been utilized for Multi-Level Thresholding particularly with PIOA to date and this paper focuses on this as one of its main contributions.
- To explore the efficacy of the hitherto untested PIOA with Tsallis and t-entropy, a meticulous comparison analysis was conducted across two image kinds, namely standard color images and pathology images.

(a)

(b)
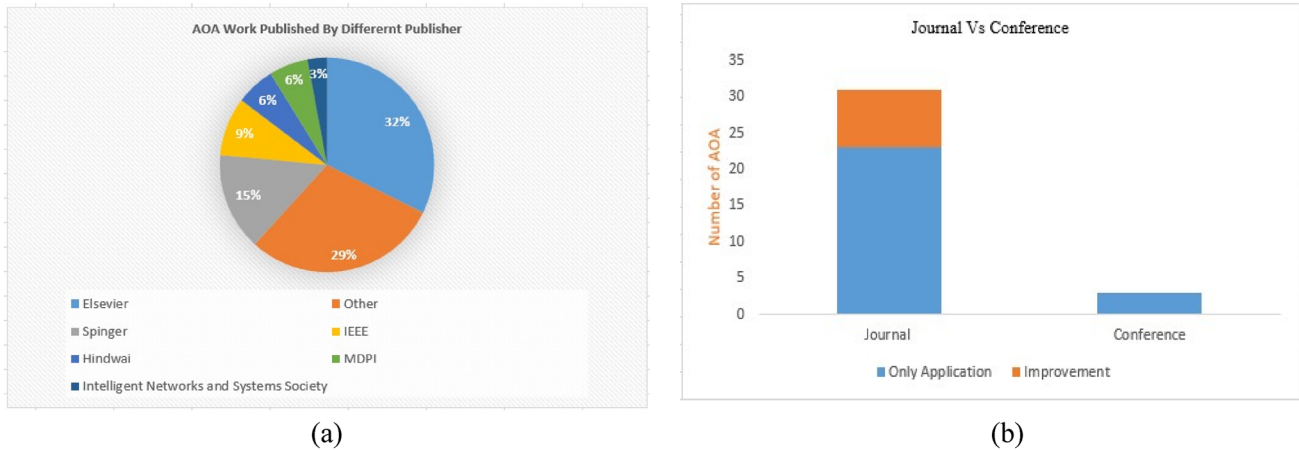
Fig. 3 **a** AOA-based work published by different publishers. **b** Number of AOA-based work published in Journal Vs Conference

Fig. 4 Application area of AOA Vs number of paper published

	Energy	Network	Medical	Image	Feature selection	Engineering	Social	Environment	Plant Disease	Human Disease	Electronics	Electrical
Number of AOA	17	3	2	4	1	3	1	1	2	2	1	2
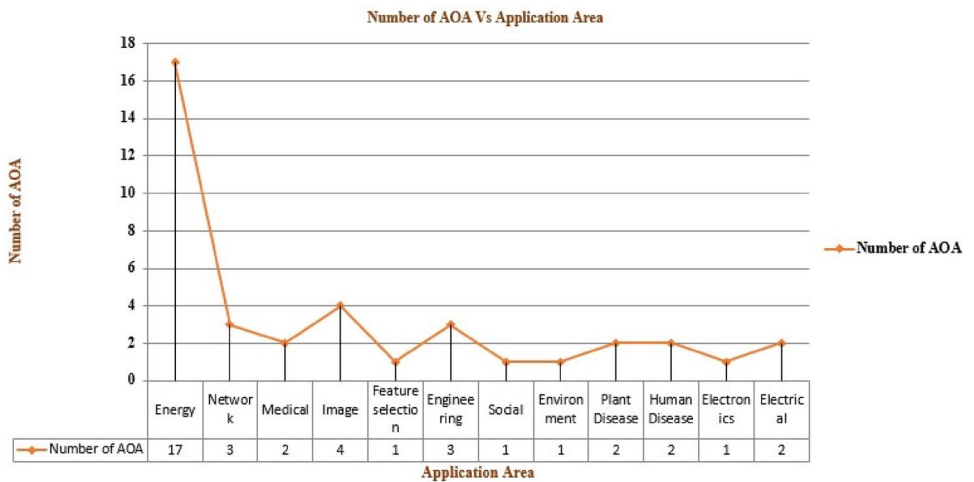
The paper's remaining sections are organized as follows: The brief discussions on AOA and improvement and application area of AOA in recent years (2020–2022). Tsallis and *t*-entropy are presented in Sect. 5. Section 6 highlights the experimental results of recently developed PIOA in the field of MLT considering Tsallis entropy and *t*-entropy as objective functions. Lastly, Sect. 7 discusses the conclusion and future directions for study.

2 Methodology

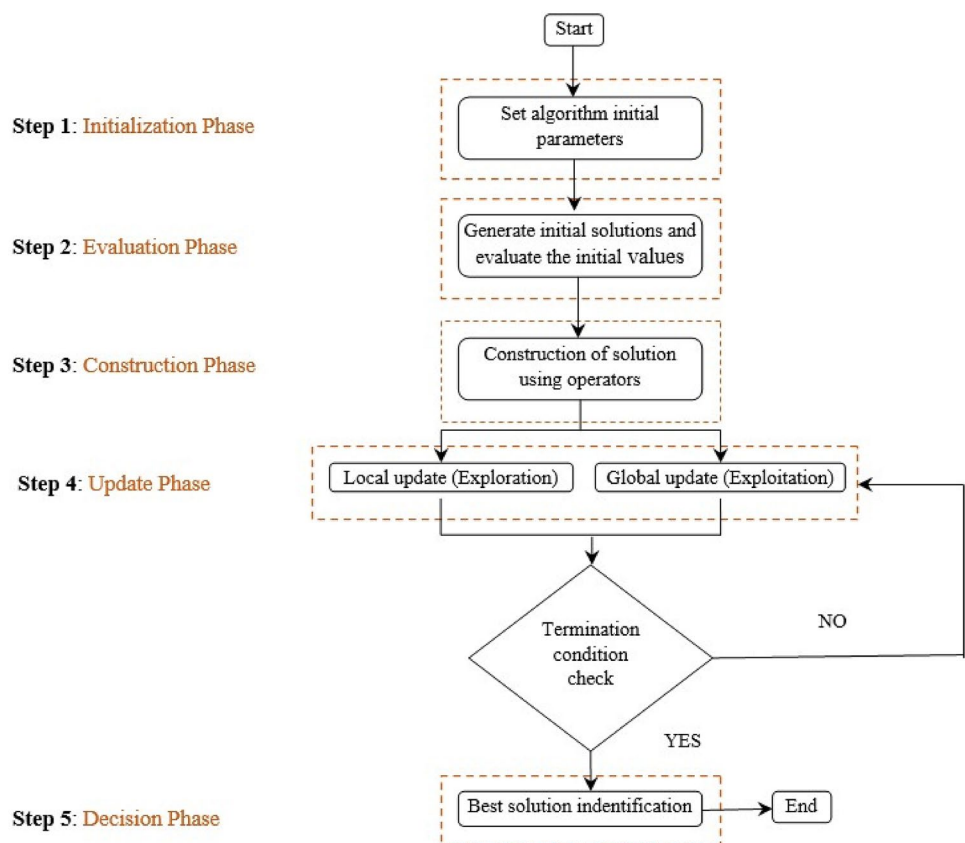For several decades, the natural phenomenon has been constantly borrowed bearing in mind its outstanding facts, functions, and phenomenon to resolve complex optimization difficulties. As with the physics-based algorithm, the motivations derived from physical laws are transformed into workable solutions and then evolve over time. To solve various optimization issues, in the last 3 years (2019 to 2021), some efficient Physics Inspired Optimization Algorithms (PIOA) have been introduced and this paper deals with the same, and also a comparative study has been done in the result section. The various PIOA have been listed in Table 1 and this section deals with the discussion on recent PIOA namely Archimedes Optimization Algorithm (AOA). Algorithm 1 is

a summary of the overall approach to MLT utilizing NIOA, which is comprised of several phases (Fig. 5).

2.1 Archimedes Optimization Algorithm (AOA)

Archimedes Optimization Algorithm [10] is a population-based PIOA algorithm that has been built upon the concept of the law of physics popularly recognized as the Archimedes principle. Archimedes' principle basically elucidates the law of buoyancy which fundamentally elaborates the association amongst an object immersed in a fluid and buoyant force that is applied to it. However, if at all the weight of the object is superior to that of the weight of the displaced fluid, the object tends to sink else, the object will float above the fluid taken into consideration. In AOA, the population individuals of the algorithm are compared and considered as the immersed objects. Since all the population-based NIOA inaugurate its search process with an initial population known as candidate solutions that are associated with some random density, volume, and acceleration. Similarly, AOA also commences with a similar concept as that of the other existing population-based algorithm wherein each of the objects, O_i that is immersed, with total population N is initialized with a random search space position with lower bound lb_i and upper bound ub_i

Fig. 5 General methodology for multilevel thresholding employing NIOA

Step 1: Initialization Phase

Step 2: Evaluation Phase

Step 3: Construction Phase

Step 4: Update Phase

Step 5: Decision Phase

which basically is the fluid here as depicted Details algorithm steps are given below.

2.2 Algorithms Steps

In this section, we present the AOA algorithm's mathematical formulations. Theoretically, AOA is a global optimization method because it consists of both exploration and exploitation phases. Pseudo-code of this algorithm presents in Sect. 2.3. The following are the AOA's mathematical equation-based steps:

2.3 Step 1: The Initialization Phase

All the parameters of AOA are initialized with help of (1)

$$O_i = rand \times (ub_i - lb_i) + lb_i; where\ i = 1, 2, 3, \ldots, N \tag{1}$$

Here, O_i is the ith object within the N (Population size). ub_i and lb_i is the upper bound and lower bounds in the search space respectively.

Each the ith object's volume (vol) and density (den) are initialized using the Eq. (2).

$$vol_i = rand \tag{2}$$

$$den_i = rand \tag{3}$$

$rand$ is a D dimensional vector, that generates random numbers between [0, 1] randomly.

Final initializes the acceleration (acc) of the ith object using (4)

$$acc_i = lb_i + rand \times (ub_i - lb_i) \tag{4}$$

In the step 2, by analyzing the original population, the best fitness values are picked and assigned it to $Xbest, den_{best}, vol_{best}$ and acc_{best}.

2.4 Step 2: Update the Volumes and Densities

For object i the density and volume are updated according following Eq. (5) in $t + 1$ iteration.

$$den_i^{t+1} = den^i + rand \times (den_{best} - den_i^t)$$
$$vol_i^{t+1} = vol^i + rand \times (vol_{best} - vol_i^t) \tag{5}$$

The vol_{best} and den_{best} represent the best volume and density value which is found so far, $rand$ is the uniform distribution value between [0,1]. Transfer operator TF is utilized in AOA to transform search from exploration to exploitation, as mentioned by (6).

2.5 Step 3: Transfer Operator and Density Factor

At first, objects bump into each other, and then, after some time, they try to reach a state of equilibrium. Transfer operator TF is used in AOA to convert search from exploration to exploitation, as stated by (6)

$$TF = \exp\left(\frac{t - t_{max}}{t_{max}}\right) \tag{6}$$

where transfer TF increases gradually over iteration until it reaches 1. Here t_{max} represent the maximum iteration and t is iteration number. In the same way, the density decreasing factor d helps AOA with global-to-local searches (7)

$$d^{t+1} = \exp\left(\frac{t_{max} - t}{t_{max}}\right) - \left(\frac{1}{t_{max}}\right) \tag{7}$$

d^{t+1} is the density of $t + 1$ iteration which decreases over time, and makes it possible to converge on a point. This density parameter plays a critical role to balance between exploitation and exploration in AOA.

2.6 Step 4.1: Exploration Phase (Collision Between Objects Occurs)

If the value of transfer operator $TF \leq 0.5$ then there is a collision between object. Then select a random material (mr) and at iteration $t + 1$, update the object's acceleration using (8).

$$acc_i^{t+1} = \frac{den_{mr} + vol_{mr} \times acc_{mr}}{den_i^{t+1} \times vol_i^{t+1}} \tag{8}$$

Here, acc_i^{t+1}, den_i^{t+1} and vol_i^{t+1} represent acceleration, density and volume of ith object in $T + 1$ iteration. den_{mr}, acc_{mr} and vol_{mr} are the density, acceleration and volume of random material. The value of TF ensure the exploration when it is ≤ 0.5. When the value of $TF \leq 0.5$ then one third of the iteration are in exploration phase.

2.7 Step 4.2: Exploitation Phase (No Collision Between Objects)

By applying the $TF \geq 0.5$ the exploration behavior changes to exploitation. That means there is no collision between object. Then the acceleration of ith object in $T + 1$ iteration updated using following Eq. (9).

$$acc_i^{t+1} = \frac{den_{best} + vol_{best} \times acc_{best}}{den_i^{t+1} \times vol_i^{t+1}} \tag{9}$$

acc_{best} is the best object's acceleration..

2.8 Step 4.3: Normalize Acceleration

When calculating percentage change, normalize the acceleration.

$$acc^{t+1}_{i-norm} = u \times \frac{acc^{t+1}_i - \min(acc)}{\max(acc) - \min(acc)} + l \qquad (10)$$

where u and l represent the normalization range and are respectively set to 0.90 and 0.10. The acc^{t+1}_{i-norm} is responsible for calculating the percentage step change for each agent. The acceleration value will be high if the item i is far from the global optimum. That means the object is in the exploration phase; otherwise, it will be in the exploration phase. In general, the acceleration factor starts with a large value and decreases with iteration.

2.9 Step 5: Update position

If $TF \leq 0.5$ (exploration phase), in next $t + 1$ iteration the ith object position calculates by following Eq. (11)

$$x^{t+1}_i = x^t_i + C_1 \times rand \times acc^{t+1}_{i-norm} \times d \times (x_{rand} - x^t_i) \qquad (11)$$

Here, C_1 represent the constant value which is equal to 2.

Otherwise, $TF \geq 0.5$ (exploitation) and update the position with the Eq. (12)

$$x^{t+1}_i = x^t_{best} + F \times C_2 \times rand \times acc^{t+1}_{i-norm} \times d \times (T \times x_{rand} - x^t_i) \qquad (12)$$

Here, C_2 represent the constant value which is equal to 6.T goes up over time and is directly related to transfer operator. The value of T defined by $T = C_3 \times TF$.

The flat F indicates a shift in motion direction by employing (13)

$$F = \begin{Bmatrix} +1 \, if P \leq 0.5 \\ -1 \, if P \geq 0.5 \end{Bmatrix} \qquad (13)$$

where $P = 2 \times rand - C_4$.

2.10 Step 6: Evaluation

Evaluate each item using the objective function f and record the best solution so far. Assign acc_{best}, vol_{best}, den_{best}, X_{best} (Fig. 6).

Fig. 6 Pseudo code of AOA
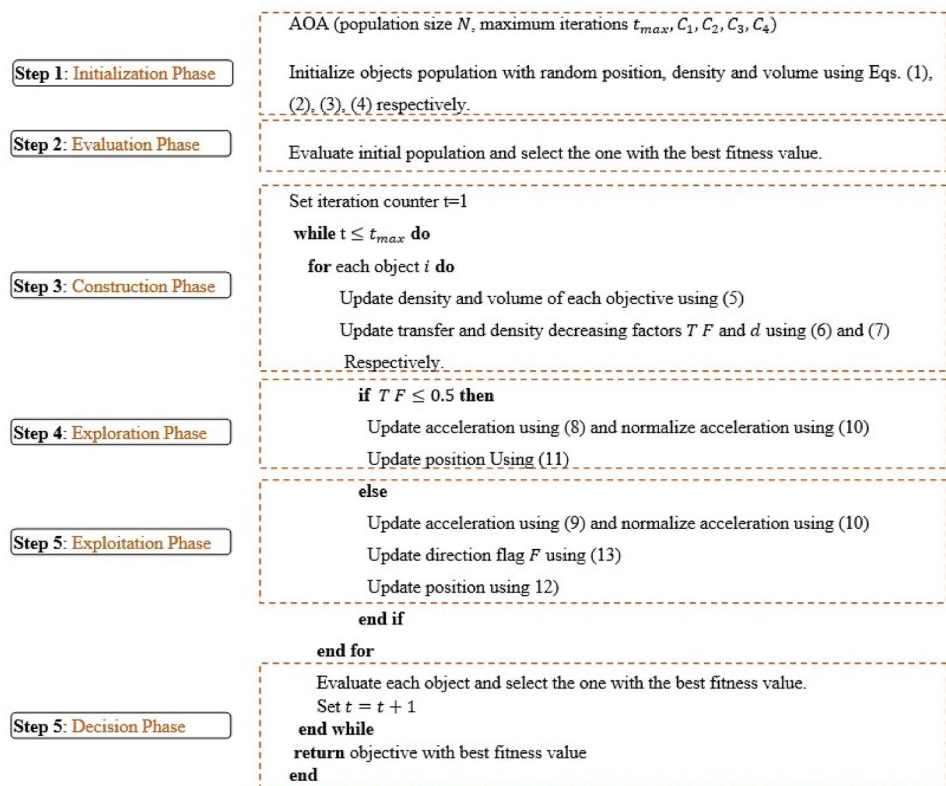
2.11 Pseudo Code of AOA

2.12 Time Complexity of AOA

The time complexity of AOA can be described as given below: Assuming the population size of the algorithm is n, the search space dimension is d, and the maximum number of iterations is T. $O(nd)$ is the calculation complexity for all of its components, including density, volume, acceleration, fitness value, and initialization. The exploration and exploitation phases update complexity are $O(T(1 + 2n + 2n \log n))$. So, applying the sum to all these complexities can be expressed as

$$O(AOA) = 5 \times O(nd) + O(T(1 + 2n + 2n \log n)) \tag{14}$$

2.13 Merits and Limitations

Most of the nature-inspired optimization problems have some shortcomings. They trap into local optima. AOA suffers also same problem and because of that finding, the optimal solution goal is not achieved. This problem increases gradually when we move from unimodal to a multimodal or high-dimension complex problem. AOA is renowned for its efficiency, simplicity, and resilience, but it also has issues with premature and sluggish convergence, which causes it to become stuck in local minima. AOA generates a new solution based on the previous iteration. This phenomenon may reduce the algorithm coverage rate and might cover the whole search space effectively and it reduces the algorithm efficiency. So many researchers introduce various methods or adapt new parameters to balance between exploration and exploitation phase. All of the enhanced versions of AOA that which author found so far are discussed below.

3 Enhanced AOA Variants

There are a numerous number of physics-inspired based meta-heuristic algorithms proposed by various researchers. Each algorithm has its advantages and drawback. AOA is one of the new physis-inspired algorithms which become very popular within a very short period. Though it has also some drawbacks but most of the cases it gives us excellent results in various real-world applications. In the energy sector, it has made a significant impact. In a few cases, it is observed that it traps in local optima due to unbalancing of exploration and exploitation phase. So, some researchers tried to make this AOA better and more robust for their

application. Sometimes an extra parameter is added [19] or a chaotic method is introduced inside the algorithm [21] or Levy Flight-based method is adopted [24] to avoid trapping into local optima. In most cases, researchers modified AOA according to their needs, and also they tried to modify the algorithm in such a way so that it can perform equally well for other applications. In this literature survey, we found that eight improvements to AOA have been proposed so far. A graph in Fig. 3b shows two things, i.e., the number of published papers in journals vs conferences and the number of improvement papers among the total proposed papers. Details study of all proposed improvement papers is given in Table 2.

4 Application of AOA

In the last twenty years, the nature-inspired optimization algorithm (NIOA) has been used in a wild variety of fields such as the energy sector, network sector, image processing field, artificial intelligence (AI), electronics sector, etc. In each sector, NIOA has put its remarkable footprint. In the last two decade, more than two hundred optimization algorithm has been proposed so far. Each algorithm has its flavor, which means the performance of these algorithms is application dependent. As previously said according to the free lunch theorem one cannot say that one algorithm gives the best result in all the fields. So, like other NIOA Archimedes Optimization Algorithm (AOA) is not the exception. This AOA has also some drawback which was discussed in the previous section and it is also been improved by many researchers. The researcher modifies the AOA according to its application area which is discussed in Table 2. From the literature survey of AOA, we can conclude that AOA has been widely used in the energy sector, especially in the wind energy domain [20, 26, 29]. AOA is also used in proton exchange membrane fuel cells [18, 21, 33] for parameter optimization. The application of AOA in the medical image domain is very little [34]. Only one paper we found where AOA has been applied in the medical image domain. In this paper, the author developed a model to detect and diagnose disease from chest X-rays. Though we found three papers in the image processing domain where AOA has been applied. Apart from medical images, AOA is also used to classify soybean plant disease [38] and Human facial analysis [35]. This paper AOA use here to determine the ideal facial area for gender recognition [35]. AOA has also been used in wireless sensor networks [22] and 5G cellular networks [46] to minimize traffic. Details study of the application area of AOA is discussed in Table 3.

Table 2 Improvements of AOA

Variant	Name	Application	Results	Author (Ref.)
I-AOA	I-AOA	PEM fuel cell parameter identification	This improved I-AOA uses two efficient strategies namely Orthogonal learning (OL) and Local escaping operator (LEO). The performance of this method was evaluated on CEC'2020 test suite and also in three engineering real word problem namely rolling element bearing, problems—tension/compression spring and pressure vessel. Author claims that this I-AOA method gives better result than original AOA	Housseinet al. [18]
AOA + Length parameter	EAOA	Feature Selection in Classification	In improve EAOA method a new parameter M_u added, this is determined by the number of steps taken by each individual. This parameter control exploitation and exploration phase. This improves method tested on twenty-three bench mark functions. Result shows that this EAOA improve exploitation competency for unimodal function and exploration capability of multimodal function. Because of its ability to avoid local optima, EAOA might outperform traditional AOA and other state-of-the-art optimizers.It was shown that the EAOA algorithm beats other well known optimizers in a statistically significant and comparable manner using the Wilcoxon rank-sum test	Desuky et al. [19]
AOA + dimension learning	IAOA	Optimal Power Flow	The dimension learning-based method is used in IAOA to enhance the object's location. For each iteration, the x i item is moved from its present location using both traditional AOA search tactics and DL strategies. Three separate power systems, the IEEE 57-bus, IEEE 30-bus, and the 16-bus South Marmara regional transmission systems, are solved using the IAOA method	Akdag [20]

Table 2 (continued)

Variant	Name	Application	Results	Author (Ref.)
AOA + 1-dimensional chaotic	IAOA	Parameters estimation of a proton exchange membrane fuel cell	In this IAOA a new 1- dimensional chaotic is introduced. This mechanism reduces the complexity of random number generation of traditional AOA. This improve IAOA used on fuel cell which is reviewable energy sources with least amount of pollution and releases water as harmless by-product. Proton-exchange membrane (PEM) fuel cells are one of the most well-known types. They have many advantages over other types. One of the biggest problems with PEMFCs is that they are expensive to build because of their catalyst. Therefore, developing these fuel cells in the most efficient way possible could be a good way to deal with this issue as much as feasible. The researchers in this study came up with a new, slightly modified model just for this purpose	Yao et al. [21]
AOA + chaotic mapping	MAOA	Wireless Sensor Networks	In MAOA, for population initialize phase a tent chaotic map is used. This improved AOA tested on seven unimodal along with six unimodal functions. The convergence speed is better than original AOA method and it also outperformed AOA, DE, PSO etc. considering optimization ability	Cheng et al. [22]
AOA + Deep Belief Network	DBN-IAOA	Proton exchange membrane fuel cell (PEMFC)	New methods for determining the optimal model for Proton Exchange Membrane Fuel Cell (PEMFC) stacks are developed using an upgraded Deep Belief Network (DBN). During the PEMFC simulation, an improved version of AOA was applied to DBN to reduce the relative error between network output data and voltage. The proposed DBN-IAOA approach was superior to the original DBN method	Sun et al. [23]

Table 2 (continued)

Variant	Name	Application	Results	Author (Ref.)
AOA + Levy Flight	LAO	Designing Microstrip Patch Antenna	The main shortcoming of AOA is it get trapped in local minima and also it has a slow convergence rate. To overcome this issue author proposed a new Levy Flight based Levy Flight Archimedes optimizer (LAO). This improves algorithm exploration efficiency which it can avoid to trap into local optima during the search. This proposed technique tested on CEC 2017 test function and also compared with well-known evolutionary algorithms. This algorithm also applied on real world problem like four different microstrip patch antenna issues and established algorithm efficiency	Singh et al. [24]
AOA + golden Levy	MSAOA	Benchmark function	A Multi-Strategy improved Archimedes Optimization Algorithm (MSAOA) was proposed to address the shortcomings of the standard Archimedes Optimization Algorithm (AOA) in solving optimization problems, such as its limited global exploration capability, slow convergence speed, and poor solution accuracy	Chen et al. [25]

4.1 Paper Sources and Keywords

(A) Sources

The mentioned papers have been collected from the following sources:

(i) SpringerLink—https://www.springerlink.com
(ii) Google Scholar—https://scholar.google.com
(iii) IEEE Xplore—https://ieeexplore.ieee.org
(iv) ScienceDirect—https://www.sciencedirect.com
(v) ACM Digital Library—https://dl.acm.org
(vi) DBLP—https://dblp.uni-trier.de
(vii) JOCA —http://www.joca.cn
(viii) WILEY—https://www.wiley.com
(ix) Taylor & Francis—https://www.tandfonline.com

(B) Keywords

Each of these above sources is queried with the following combinations of keywords:

KW1: Nature-Inspired Optimization Algorithms.

KW2: Image segmentation.

KW3: Hierarchical and Partitional clustering based image segmentation.

KW4: Nature Inspired Optimization Algorithm based image clustering.

KW5: Image segmentation medical image.

KW6: Image segmentation pathology image.

KW7: optimization.

KW8: Physics Inspired Optimization Algorithms.

KW9: Archimedes Optimization Algorithm.

KW10: Image segmentation using Swarm Intelligence algorithms.

KW11: Archimedes Optimization Algorithm improvement.

KW12: Multi-thresholding.

KW13: Archimedes Optimization Algorithm in Multi-thresholding.

5 AOA-Based Image Multi-level Thresholding

There are several computer vision applications in which image segmentation is a fundamental part of the process and thresholding is regarded as extremely important in this sector. Based on the number of threshold values one may classify two types of thresholding, namely bi-level and multi-level thresholding. From its name, one can say that when there is two threshold value then it is the bi-level threshold and when the threshold value is more than two

Table 3 Application area of AOA

Publisher	Name	Application	Results	Author (Ref.)
Applied Energy (Elsevier)	Ensemble wind speed forecasting with multi-objective Archimedes optimization algorithm and sub-model selection	Wind speed forecasting	Using AOA, one may make precise and dependable forecasts of wind speed. The author proposes a new decomposition–forecasting–optimization ensemble system (DFOES) to close the forecasting gap. interval forecasting (IF), data decomposition, ensemble point forecasting (PF), sub-model selection, and model assessment are the five modules of this model approach	Zhang et al. [26]
Ain Shams Engineering Journal (Elsevier)	A novel distributed generation planning algorithm via graphically-based network reconfiguration and soft open points placement using Archimedes optimization algorithm	Build a network for optimal distribution of power	AOA is used to maximize the hosting capacity (HC) by reconfiguring the network in steps, then putting in soft open points (SOPs). This maximization of HC is formulated as a multi-objective optimization problem. This proposed model ensures better load balancing between distribution feeders and minimizes power loss	Ali et al. [27]
IOP Publishing	Comprehensive optimization of distributed generation considering network reconstruction based on Archimedes optimization algorithm	Network reconfiguration of distribution automation of power	This paper does extensive research and analysis on the best way to set up distributed generation (DG), taking into account how the network is reconfiguration which can reduce the power loss. Configuring DGs and networks involve solving large-scale nonlinear optimization issues, which have been widely researched in the literature	Li et al. [28]
Ain Shams Engineering Journal (Elsevier)	Archimedes optimization algorithm based maximum power point tracker for wind energy generation system	Maximum power point tracker (MPPT) to ensure maximum wind energy generation	For the wind energy producing system, AOA is used to simulate the MPPT (Maximum Power Point Tracking). A WT is linked to a PMSG in the setup described above. For precise control of the amount of DC power required by the load, the output of the generator is converted from AC to DC using a 3-phase rectifier and a boost converter. MOSFET duty cycle is regulated by AOA in order to maximize wind energy production system performance	Fathy et al. [29]

Table 3 (continued)

Publisher	Name	Application	Results	Author (Ref.)
Solar Energy (Elsevier)	An efficient photovoltaic modeling using an Adaptive Fractional-order Archimedes Optimization Algorithm: Validation with partial shading conditions	Optimal parameters of the photovoltaic (PV) models	According to the author, the optimal photovoltaic (PV) model parameters may be determined using a novel approach based on fractional calculus. An Adaptive Fractional-order Archimedes Optimization Algorithm (A-FAOA) was used to identify the model parameters for several photovoltaic solar cells/modules under various environmental conditions	Yousri et al. [30]
Intelligent Networks and Systems Society	Intelligent Control of Power System Stabilizer Based on Archimedes Optimization Algorithm—Feed Forward Neural Network	Power System Stabilizer	The author combines AOA and neural network (NN) to create an improved version of AOA-NN. The goal of the research is to come up with a hybrid AOA-NN method to make power system stabilizers work better. Experimental results outperformed FFNN, CFNN, DTDNN, and STSA-NN method	Aribowo et al. [31]
Measurement (Elsevier)	Adaptive variational mode decomposition based on Archimedes optimization algorithm and its application to bearing fault diagnosis	Rotating machinery fault diagnosis	Variational mode decomposition (VMD) is frequently employed in rotating equipment fault diagnostics. It is a widely used method all over the world. The selection of appropriate parameters is always based on experience. To overcome this issue and tune the proper parameter AOA is used by the author. This proposed method gives a better result to extract the fault characteristics	Wang et al. [32]

Table 3 (continued)

Publisher	Name	Application	Results	Author (Ref.)
Energy (Elsevier)	Recent approach based heterogeneous comprehensive learning Archimedes optimization algorithm for identifying the optimal parameters of different fuel cells	Performance analysis of fuel cell	The author proposed heterogeneous comprehensive learning Archimedes optimization algorithm (HCLAOA) to design a new model for performance analysis of fuel cells (FCs) that estimates FCs character properly. This model was used on Proton Exchange Membrane Fuel Cell (PEMFC) and Solid Oxide Fuel Cell (SOFC) and done extensive testing on different conditions which outperformed state of art algorithms like Slap Swarm Optimization Algorithm (SSOA), Atom search Optimizer (ASO), etc	Fathy et al. [33]
Computational Intelligence and Neuroscience (Hindawi)	A New Optimal Diagnosis System for Coronavirus (COVID-19) Diagnosis Based on Archimedes Optimization Algorithm on Chest X-Ray Images	Coronavirus (COVID-19) Diagnosis from X-ray images	COVID-19 is a member of the coronavirus family and has emerged as a fetal disease in recent years. In this paper, the author developed a model to detect and diagnose disease from chest X-rays. The author utilized AOA to extract features from X-ray images. Autor asserts that this model has an accuracy of 86% and a precision of 96%	Chen and Rezaei [34]
Soft Computing (Springer)	An Intelligent handcrafted feature selection using Archimedes optimization algorithm for facial analysis	Human facial analysis	Due to recent advancements in technology and mobile applications, computer vision researchers are increasingly interested in human face analysis (HFA). AOA use here to determine the ideal facial area for gender recognition. Authors claim that the suggested technique outperforms convolutional neural network (CNN) with Gallagher's dataset accuracy of 96.08 percent	Neggaz and Fizazi [35]

Table 3 (continued)

Publisher	Name	Application	Results	Author (Ref.)
International Conference on Digital Technologies and Applications (Springer)	Multi-objective Archimedes Optimization Algorithm for Optimal Allocation of Renewable Energy Sources in Distribution Networks	Reduce total power losses and total voltage deviation	This study makes use of the Archimedes Optimization Algorithm (AOA) to locate the most optimal distribution network (DN) allocation for distributed generation (DG); (AOA). Power losses and voltage variation are reduced. Power losses are reduced and the voltage profile is improved when DG units are assigned to distribution networks. The PSO-like method was shown to be outperformed by the new approach	Eid and El-Kishky [36]
Resbee Publisher	Archimedes Optimization Algorithm: Heart Disease Prediction	Heart disease prediction	The author attempted to forecast heart problems using a database of heart-related issues using a neural network for feature detection. The author employed AOA to optimize the weights of NN. The suggested method's results show that it is more effective than the other traditional approaches available	Anand [37]
Wireless Personal Communications (Springer)	A Cloud-Based Platform for Soybean Plant Disease Classification Using Archimedes Optimization Based Hybrid Deep Learning Model	Soybean Plant Disease	To classify bean diseases, the author developed a hybrid deep learning model with an Archimedes optimization method (HDL–AOA). Here author tried to classify Rhizoctonia root rot, Bean halo blight, and Pythium diseases like diseases. The suggested model achieves a lower Mean absolute percentage error (MAPE) than many other existing techniques	Annrose et al. [38]
MDPI	Stability Enhancement of Wind Energy Conversion Systems Based on Optimal Superconducting Magnetic Energy Storage Systems Using the Archimedes Optimization Algorithm"	Wind energy storage system	The author used AOA to enhance the performance of wing energy conversion system stability which was integrated with the superconducting magnetic energy storage (SMES) system. The SMES system has a significant influence on the integration of wind generators with the electrical grid by controlling wind generator output and enhancing the operation of the power system	Abdelbadie et al. [39]

Table 3 (continued)

Publisher	Name	Application	Results	Author (Ref.)
MDPI	"Archimedes Optimization Algorithm Based Selective Harmonic Elimination in a Cascaded H-Bridge Multilevel Inverter	Removing selected harmonics from a cascaded H-bridge (CHB) multilevel inverter (MLI)	This work describes the Archimedes optimization approach for removing selected harmonics from a cascaded H-bridge (CHB) multilevel inverter (MLI). The primary goal of selective harmonic elimination (SHE) is to remove lower-order harmonics in 5-level, 7-level, and 9-level inverters by determining the best switching angle	Khan et al. [40]
Clean Energy	Optimal allocation of solar photovoltaic distributed generation in electrical distribution networks using Archimedes optimization algorithm	Electrical distribution networks	This research proposes to use a unique Archimedes optimization method to determine the ideal placements and sizes of solar photovoltaic (SPV) systems in electrical distribution networks. It minimizes dependency on the grid and, as a result, it also reduces traditional power generation's greenhouse gas emissions. The author claims that this proposed model outperformed several nature-inspired meta heuristic methods	Janamala and Radha [41]
Research Square	Soybean Plant Disease Classification using Archimedes Optimization Algorithm based Hybrid Deep Learning Model	Soybean Plant Disease Classification	In this paper for bean disease classification, the author developed a hybrid deep learning model with an Archimedes optimization method (HDL-AOA). Experimental result shows that this model has lower MAPE other than some existing methods. It has also excellent sensitivity, accuracy, precision, and F-score	Annrose et al. [42]
Journal of Cleaner Production (Springer)	Predicting municipal solid waste using a coupled artificial neural network with Archimedes optimization algorithm and socioeconomic components	Solid Waste prediction	This work examines the implementation of optimized ANN models for forecasting monthly SW generation in Iran utilizing information pertaining to seven Iranian megacities. The author used different nature-inspired algorithms such as PSO, GA, etc. for the aim of tanning the ANN model, however, ANN-AOA excelled them all with an RMSE of 73%	Liang et al. [43]

Table 3 (continued)

Publisher	Name	Application	Results	Author (Ref.)
intelligent automation and soft computing (Tech science press)	Design of Optimal Controllers for Automatic Voltage Regulation Using Archimedes Optimizer	Controllers for Automatic Voltage Regulation	In this work, the author recommends employing an AOA to fine-tune the proportional–integral–derivative (PID) controller settings for Automatic voltage regulators (AVRs) The usefulness of employing an AOA to optimize the settings of a fractional-order PID (FOPID) controller and a PID plus second-order derivative (PIDD2) controller for AVRs are also tested. This proposed method compared with other algorithms and the result clearly indicate that AVRs with the AOA-PID controllers outperformed all other results	Agwa et al. [44]
IEEE Xplore	"Power System Harmonics Estimation using Hybrid Archimedes Optimization Algorithm-based Least Square Method"	Estimating harmonics of a power system	This research presents a hybrid method known as the Archimedes optimization algorithm-based least square (AOA-LS) technique for estimating the harmonics of a power system. AOA-LS method is examined and compared to three other techniques: FA-LS, PSOPC-LS, and (ABC-LS). According to the results, the suggested approach outperforms all other algorithms in terms of estimation precision and processing time	Apon et al. [45]
International Journal of Power Electronics and Drive Systems	Optimal sizing and sitting of electric vehicle charging station by using Archimedes optimization algorithm technique	Optimal sizing and sitting of electric vehicle charging station	This research offers an optimization model for the ideal construction of a grid-connected electric vehicle (EV) extreme fast charging station, taking into account the integration of PV and energy storage. Using the suggested approach, the yearly net cost of the extremely fast charging station may be minimized (i.e., the annualized net profit can be maximized)	Zaki et al. [46]

Table 3 (continued)

Publisher	Name	Application	Results	Author (Ref.)
IEEE Xplore	Archimedes Optimization Algorithm with Deep Belief Network Based Mobile Network Traffic Prediction for 5G Cellular Networks	Mobile Network Traffic Prediction for 5G	This study Offer on the development of the Archimedes Optimization Algorithm with the Deep Belief Network-based mobile network traffic prediction (AOADBN-MTP) model for 5G cellular networks. This model consists of 3 stages such as pre-processing, prediction and hyperparameter tuning. Results from the simulations showed that the AOADBN-MTP approach was improved, with an average MAPE of 0.034 and a running duration of 0.1373 s	Selvamanju and Shalini [47]
Turkish Journal of Electrical Power and Energy Systems	Enhancement of Transmission System Security with Archimedes Optimization Algorithm	Transmission system management	In this work, the innovative Archimedes optimization algorithm (AOA) is used instead of deterministic techniques to tackle the bus splitting optimization (BSO) issue. The BSO is a technique that preserves system security by allocating transmission feeders to appropriate busbars. The results of the author's implementation reveal that the AOA algorithm is effective and resilient enough to address the BSO problem in the Turkish Electricity Transmission System's Istanbul Anatolian Region and to improve power system security	Doğan and Yörükeren [48]

Table 3 (continued)

Publisher	Name	Application	Results	Author (Ref.)
Journal of Optoelectronics Laser	Archimedes Optimization Algorithm based Fractional MPPT for Enhancing Performance and Efficiency of Photovoltaic Systems	Enhancing Performance and Efficiency of Photovoltaic Systems	For photovoltaic (PV) systems, this research focuses on the problem of maximum power point tracking (MPPT). The primary disadvantages with traditional MPPT include slower reaction owing to a fixed step change, excessive ripple, and increased oscillation due to maximum power point swing (MPP). This study proposes the fractional optimizer MPPT to address these problems. Using Archimedes optimization algorithm (AOA), the FOPID controller's five parameters may be fine-tuned to achieve optimum performance	Hannon et al. [49]

it is said multi-level threshold. Multilevel Thresholding (MLT) segmentation algorithms have limits while looking for ideal thresholding values comprehensively to enhance the objective function, which also increases computing cost. In a nutshell, as the number of thresholds increases, MLT approaches become increasingly computationally difficult. Many scholars are drawn to a variety of methods that are inspired by nature or human behavior or physics phenomenon that may be used extensively to address this and other concerns with MLT.

In addition to that recently designed PIOA has also been utilized for MLT in the last 2 to 3 years. However, the effort is too little. For example, Dinkar et al. [50] suggested an Opposition-Based Laplacian Equilibrium Optimizer (OB-L-EO) in Image Segmentation using Multilevel Thresholding by utilizing Otsu's interclass variance function over Standard Gray Scale Images and employing Berkeley Segmentation Dataset (BSD) and claims that the Proposed OB-L-EO is capable of exhibiting superior outcome in terms of maximizing variance and PSNR values thereby outperform other methods. Basset et al. [51] proposed an Equilibrium Optimization Algorithm (EOA) for multi-thresholding image segmentation by utilizing Kapur's entropy over Standard Gray Scale Images and employing Berkeley Segmentation Dataset (BSD) and claims proposed EOA is capable of outperforming all other algorithms. However, EO failed to show its superiority over some algorithms in Standard values, and CPU time for the large threshold levels. Qi et al. [52] proposed Hybrid Equilibrium Optimizer Algorithm (HEOA) for multi-level image segmentation utilizing 3D Otsu over Standard Color Images, and Color Satellite Images using the CEC2015 dataset and claims that the proposed HEOA is capable of performing better (has the good optimal ability) than the other methods. However, it takes enormous time to iterate in order to find the best solution. On the other hand, this method has strong performance in wood fiber image segmentation thereby having a greater scope in the field of medical image segmentation, forest fire image segmentation, and so on. Rai et al. [7] also performed a comparative study among six NIOA called Archimedes Optimization Algorithm (AROA), Aquila Optimizer (AQO), Arithmetic Optimization Algorithm (AOA), Rat Swarm Optimization Algorithm (RSA), Particle Swarm Optimization (PSO), and Firefly Algorithm (FA) in satellite image MLT domain by considering Masi entropy as an objective function. Experimental results showed that AROA gave better results than other tested NIOA in terms of optimization ability, quality parameters, and execution time. Kurban et al. [53] also performed a comparative study among six novel NIOA such as Slime Mould Algorithm (SMA), Henry Gas Solubility Optimization (HGSO), turbulent flow of water-based Optimization (TFWO), Political Optimizer (PO), Marine Predators Algorithm (MPA) and Equilibrium Optimization (EO) for

color image thresholding using Kapur and Otsu as objective functions. Comprehensive studies showed that MPA and TFWO produced better results than SMA, EO, PO, and HGSO for satellite images. Cuckoo search-based multi-level thresholding for lymphoblastic leukemia image segmentation proposed by Ray et al. [54]. The next section focuses mostly on the problem foundation and objective function for multi-level thresholding.

5.1 Problem Formulation of Multilevel Thresholding

In image segmentation, based on multiple thresholding [55, 56], the primary objective is to choose threshold values so that the segmented images possess the required characteristic. Here the threshold values are taken into account while constructing the objective function. By minimizing or maximizing of objective function with help of threshold value we can achieve our goal.

Suppose, an image I have L gray levels and which can be classified into K number of classes i.e. $(C_1, C_2, \ldots, C_i, \ldots, C_k)$ using $(K-1)$ number of thresholds which values are $(T = t_1, t_2, \ldots, t_i, \ldots, t_{K-1})$, where $(t_1 < t_2 <, \ldots, < t_i, \ldots, < t_{K-1})$. Here, for an 8-bit image, $L = 256$ and the grayscale levels fall between 0 and 255. So, a pixel with gray level G belongs to the class C_i if $(t_{i+1} < G < t_i)$ for $i = 1, 2, \ldots, K$. So, a single objective function can be written as

$$T' = \arg \max/\min_{0 \leq T \leq L-1} \{F(T)\} \tag{15}$$

Here thresholds T′ which optimizes the objective function F(T). To get the segmented image I, the objective function $F(T)$ must satisfy the desired property. Following is a simple mathematical implementation of Tsallis entropy as an objective function in this study.

For multi-objective thresholding, T'' optimize the set of objective functions.

$$F(T) = \left(F_1(T), F_2(T), \ldots, F_{j-1}(T), \ldots, F_n(T) \right), where \, n > 1 \tag{16}$$

$$T'' = \arg \max/\min_{0 \leq T \leq L-1} \{F(T)\} \tag{17}$$

5.2 Objective Function

5.2.1 Tsallis Entropy as Objective Function

Constantin Tsallis introduced the Tsallis entropy as an extension of the Boltzmann–Gibbs entropy measure [57]. Using the entropy formula given in Eq. (18) Tsallis' entropy

measure may be expanded to a non-extensive system based on the idea of multi-fractal theory.

$$S_q = \frac{1 - \sum_{i=1}^{k} (p_i)^q}{q - 1} \tag{18}$$

where, $0 \leq p_i \leq 1$ represents the probability of the state i. In the case of a gray level image, It indicates the appearance of the ith gray level in a grayscale image. The Tsallis parameter q represents the system under consideration's non-extensivity. Using the pseudo-additivity entropy rule, it may be expressed as

$$S_q(f + b) = S_q(f) + S_q(b) + (1 - q).S_q(f).S_q(b) \tag{19}$$

Here, the threshold value t separates the image's foreground and background classes, which are represented by the, f and b.

Here, classes f and b are used to represent the image's foreground and background areas, which are separated from one another by the image's threshold value (t). Suppose, $\{(p_1, p_2, \ldots, p_L) | p_i \geq 0, i = 1, 2, \ldots, L.;$ L = number of discrete gray levels; $\sum_{i=1}^{n} p_i = 1\}$ is the probability distribution of the image's gray-level intensities. The following equation represents the probability distribution of classes f and b:

$$P_f = \frac{p_1}{P^f}, \frac{p_2}{P^f}, \ldots, \frac{p_t}{P^f} \text{ and } P_b = \frac{p_{t+1}}{P^b}, \frac{p_{t+2}}{P^b}, \ldots, \frac{p_L}{P^b} \tag{20}$$

where,

$$P^f = \sum_{i=1}^{t_1} p_i, \text{ and } P^b = \sum_{i=t+1}^{L} p_i \tag{21}$$

Therefore, for each class, Tsallis entropy may be expressed as follows:

$$S_q^f(t) = \frac{1 - \sum_{i=1}^{t} (p_i/P^f)^q}{q - 1}, \; S_q^b(t) = \frac{1 - \sum_{i=t+1}^{L} (p_i/P^b)^q}{q - 1} \tag{22}$$

Bilevel-thresholding maximizes the total of the information measures for the foreground and background. Therefore, the following formulation may be used to determine the appropriate threshold:

$$t_{opt} = \text{Arg max} \left[S_q^f(t) + S_q^b(t) + (1 - q).S_q^f(t).S_q^b(t) \right] \tag{23}$$

Subject to the following constraints:

$$\left| P^f + P^b \right| - 1 < S < 1 - \left| P^f + P^b \right|,$$
$$\text{where, } S(t) = S = S_q^f(t) + S_q^b(t) + (1 - q).S_q^f(t).S_q^b(t) \tag{24}$$

The following expression may be used to simply expand this approach to multi-level thinking:

$$(t_1, t_2, \ldots \ldots, t_m)$$
$$= \text{Arg max} \left[S_q^1(t) + S_q^2(t) + \cdots + S_q^M(t) + (1-q).S_q^1(t).S_q^2(t) \ldots .. S_q^M(t) \right] \quad (25)$$

where,

$$S_q^1(t) = \frac{1 - \sum_{i=1}^{t_1} \left(p_i / P^1 \right)^q}{q-1}, \text{ and}$$
$$S_q^M(t) = \frac{1 - \sum_{i=t_m+1}^{L} \left(p_i / P^M \right)^q}{q-1}, \text{ And } M = m+1 \quad (26)$$

Subject to the following constraints:

$$\left| P^1 + P^2 \right| - 1 < S^1 < 1 - \left| P^1 + P^2 \right|, \left| P^2 + P^3 \right| - 1 < S^2 < 1 - \left| P^2 + P^3 \right|$$
$$\& \left| P^m + P^{m+1} \right| - 1 < S^M < 1 - \left| P^m + P^{m+1} \right| \quad (27)$$

where P^1, P^2 and P^{m+1} corresponding to S^1, S^2 and S^M have been computed using $t_1, t_2, \ldots \ldots, t_m$ respectively.

5.2.2 t-Entropy as Objective Function

In 2021, Chakraborty et al. introduced a new measure of entropy termed t-entropy [17]. Suppose there is an image I which has a normalized histogram $\boldsymbol{p} = (p_0, p_2, p_3, \ldots, p_n, \ldots, p_{L-1}) | p_i \geq 0, i = 0, 1, 2, \ldots, n, \ldots L - 1$; in where L is the image's number of gray levels and $\sum_{i=0}^{L-1} p_i = 1$, then t-entropy (H_c) of the image is then calculated as follows:

$$H_c(\boldsymbol{p}) = \sum_{i=0}^{L-1} p_i \tan^{-1} \left(\frac{1}{p_i^c} \right) - \frac{\pi}{4} \quad (28)$$

where c is a positive constant.

Assuming that the normalized histogram is divided into K classes by $nt = K - 1$ thresholds(t), the entropy for each class may be determined as follows:

$$H_c^1(th_1) = \sum_{i=0}^{th_1-1} \frac{p_i}{w_1} \tan^{-1} \left(\frac{1}{\left(p_i / w_1 \right)^c} \right) - \frac{\pi}{4}$$
$$H_c^2(th_2) = \sum_{i=th_1}^{th_2-1} \frac{p_i}{w_2} \tan^{-1} \left(\frac{1}{\left(p_i / w_2 \right)^c} \right) - \frac{\pi}{4}$$
$$\vdots$$
$$\vdots$$
$$H_c^K(th_{nt}) = \sum_{i=th_{nt}}^{L-1} \frac{p_i}{w_{nt}} \tan^{-1} \left(\frac{1}{\left(p_i / w_{nt} \right)^c} \right) - \frac{\pi}{4} \quad (29)$$

where,

$$w_1(th_1) = \sum_{i=0}^{th_1-1} p_i, w_2(th_2)$$
$$= \sum_{i=th_1}^{th_2-1} p_i, \ldots \ldots \ldots \ldots, w_K(th_{nt}) = \sum_{i=th_{nt}}^{L-1} p_i \quad (30)$$

where, for ease of computation, two dummy thresholds $th_0 = 0, th_{nt} = L - 1$ are introduced with $th_0 < th_1 < \ldots < th_{n-1} < th_{nt}$. Then, the best threshold value may be determined by using this method.

$$\varphi(th_1, th_2, \ldots \ldots, th_{nt})$$
$$= \text{Arg max} \left(\left[H_c^1(th_1) + H_c^2(th_2) + \ldots + H_c^K(th_{nt}) \right] \right) \quad (31)$$

For image segmentation based on multi-level thresholding-based, the positive constant c had been evaluated over [0.01, 20] and determined to be optimal at $c = 0.1$.

6 Experimental Result

In this section, the author did a comparative study between AOA with six other PIOA with help of Tsallis entropy and t-entropy over standard pathology images and standard color images. The six PIOA's experimental results in multi-threshold domains namely Nuclear Reaction Optimization (NRO), Atom Search Optimization (ASO), Equilibrium Optimizer (EO), Henry Gas Solubility Optimization (HGSO), Flow Direction Algorithm (FDA), Atomic Orbital Search (AOS) are compared with Archimedes Optimization Algorithm (AOA). The algorithms parameter values used in these seven algorithm are defined in Table 4. Each NIOA's specifications are determined after extensive testing. Tsallis' and t-entropy are used as objective functions in the experiment. To make fair comparisons amongst NIOA techniques, the optimization procedure for each of the evaluated objective functions uses *NFE*(Number of Function Evaluations) = 1000*d as the halting condition. This criterion has been established to promote consistency with earlier published studies. When evaluating the experiments, the number of threshold values (TH) set to 4, 6, and 8 is taken into account. In addition, *FE* is a key performance metric used to evaluate the NIOA's efficiency. FE allows some technical variables, such as the computer system where experiments are performed and implemented, that affect CPU time, focusing exclusively on the algorithm's ability to explore the solution space. Mean fitness $\left(\bar{f} \right)$ and standard deviation (σ) have been used to figure out how well the PIOA can optimize. A number of other metrics were used to assess the efficiency of these PIOA-based models segmented data: the PSNR, QILV, and Feature Similarity Index, for example (FSIM). Within the realm of image segmentation, these parameters have a great deal. The list of segmentation quality metrics that are being employed is presented in Table 5. [2, 58]. The hardware and software requirements for the

Table 4 Parameter setting of the PIOA

Algorithms	Parameters	Description	Value initialized
Archimedes Optimization Algorithm (AOA)	N	Population size	50
	C_1	Control variable$_1$	2
	C_2	Control variable $_2$	6
	C_3	Control variable $_3$	2
	C_4	Control variable $_4$	0.5
Flow Direction Algorithm (FDA)	A	Population size	50
	B	Number of neighbors	1
Equilibrium Optimizer (EO)	N	Number of particles (population size)	50
	GP	Generation probability	0.5
	a_1	Constant value to control exploration ability	2
	a_2	Constant value to control exploitation ability	1
Atom Search Optimization (ASO)	K	Atom population size	50
	a	Depth weight	50
	β	Multiplier weight	0.2
Henry Gas Solubility Optimization (HGSO)	N	Population size	50
	j	Cluster number	5
	C_1	Constant [Escaping from local optima]	0.1
	C_2	Constant [Escaping from local optima]	0.2
	β	Constant [Updating Position]	1
	α	Influence of other gases in a cluster	1
	K	Constant [Updating Solubility]	1
Atomic Orbital Search (AOS)	M	Electron population size	50
	α	Random number	[0, 1]
	β	Random number	[0, 1]
	γ	Random number	[0, 1]
	φ	Random number	[0, 1]
Nuclear Reaction Optimization (NRO)	N	Nuclei population size	50
	$freq$	frequency of the sinusoidal function	0.5
	P_{Fi}	Nuclear fission probability	0.75
	P_β	β decay Probability	0.1

Table 5 Three well-known performance parameters for the evaluation of the image segmentation methods

Sl	Parameters	Formulation	Remarks
1.	Feature Similarity Index (FSIM)	$FSIM = \dfrac{\sum_{x \in \Omega} S_L(x).PC_m(x)}{\sum_{x \in \Omega} PC_m(x)}$	Defines the quality score that measures the significance of a local structure. The better the outcome, the greater the value
2.	Peak Signal to Noise Ratio (PSNR)	$PSNR = 10 log_{10} \dfrac{(2^b-1)^2}{\sqrt{MSE}}$	Represents the ratio between a signal's highest possible power and the noise power. A high PSNR indicates a favorable outcome
3.	Structural Similarity Index (SSIM)	$SSIM = \dfrac{\left(2 \times \bar{X} \times \bar{Y} + c_1\right) \times \left(2 \times \sigma_{XY} + c_2\right)}{(\sigma_X^2 + \sigma_Y^2 + c_2) \times \left(\bar{X}^2 + \bar{Y}^2 + c_1\right)}$	Determines whether a segmented image and an uncompressed or distortion-free image are similar. A higher SSIM score denotes a better outcome

experiment include MatlabR2018b and Windows-10 operating system, $\times$64-based personal computer, Ryzen 5 central processing unit, and 16 gigabytes of RAM. A standard set of 100 color photos is used to test the suggested methods which are collected from [59] (https://lear.inrialpes.fr/~jegou/data.php).

The renal pathology images are taken from [60] (https://tcgadata.nci.nih.gov/tcga/). Figure 7 depicts the original color standard picture and kidney pathology imaging.
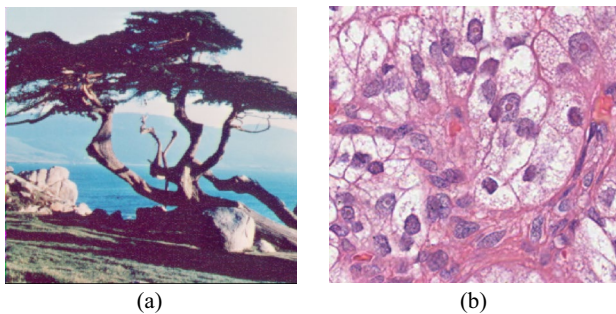
Fig. 7 Original image: **a** Standard Color Image; **b** Color Renal Pathology Image

6.1 Experimental Results of Standard Color Images over Tsallis Entropy

For the standard color picture, Fig. 8 shows the segmented results of Fig. 7a using Tsallis entropy as an objective function across **4, 6, and 8 thresholds** using different PIOA (AOA, ASO, HGSO, EO, AOS, FDA and NRO). Table 6 compares numerically the aforementioned PIOAs using Tsallis entropy as the objective function across **4, 6, and 8 thresholds** for a typical color image. Here standard deviation (σ_f), fitness function $(\bar{f})$, Computational time (Time (sec)), PSNR, FSIM and SSIM used as numerous parameters for performance evaluation of segmented image. With addition, the bold value in this table is represented the best performance value. Table 6 reveals that AOA achieves the best outcome across all **threshold values (4, 6, and 8)** for every parameter considered, but NRO achieves the lowest result across all evaluated PIOAs. From the same table, Table 6, we can conclude that when the number of thresholds increases, FSIM, PSNR, and SSIM values similarly increase for the objective function studied in this situation. The fitness value of AOA is compared to that of other PIOAs studied (Table 1) using a non-parametric significance test known as Wilcoxon's rank test [61] that permits the estimation of differences between the outcomes of two related approaches. A p value of less than 0.05 (5 percent significance threshold) strongly supports the rejection of the null hypothesis, indicating that the results of the best algorithm differ statistically insignificantly from those of the other peer algorithms and that the difference is not attributable to random chance. Table 7 presents the pair-wise comparisons of PIOA (AOA vs. ASO; AOA vs. FDA; AOA vs. EO; AOA vs. HGSO; AOA vs. AOS; and AOA vs. NRO) based on Wilcoxon p-values for Standard Color images for Tsallis Entropy for **4, 6, and 8 thresholds**. The fact that all Wilcoxon p-values collected and projected in Table 7 are less than 0.05 (5 percent significance threshold) with h = 1 is evidence against the null hypothesis, implying that the AOA fitness values for

performance are statistically superior. This suggests that AOA combined with Tsallis entropy as an objective function is competent enough to produce consistent solutions regardless of the threshold settings.

6.2 Experimental Results of Pathology Images over Tsallis Entropy

For the pathology images, Fig. 9 shows the segmented results of Fig. 7(b) using Tsallis entropy as an objective function across **4, 6, and 8 thresholds** using different PIOA (AOA, ASO, HGSO, EO, AOS, FDA and NRO). Tsallis entropy is used as the objective function in the numerical comparison of various PIOAs for pathology images with **4, 6, and 8 thresholds** in Table 8. Here standard deviation (σ_f), fitness function $(\bar{f})$, Computational time (sec), PSNR, FSIM and SSIM used as numerous parameters for performance evaluation of segmented image. With addition the bold value in this table is represented the best performance value. Table 8 reveals that AOA achieves the best outcome across all **threshold values (4, 6, and 8)** for every parameter considered, but NRO achieves the lowest result across all evaluated PIOAs. Table 8 further shows that when the number of thresholds increases, values for PSNR, FSIM, and SSIM likewise increase for the objective function studied in this situation. Table 9 displays the pair-wise comparisons of PIOA (AOA vs. ASO; AOA vs. FDA; AOA vs. EO; AOA vs. HGSO; AOA vs. AOS; and AOA vs. NRO) based on Wilcoxon p-values for Pathology images for Tsallis Entropy for **4, 6, and 8 thresholds**. All of the Wilcoxon p-values found and shown in Table 9 are less than 0.05, which is the 5 percent significance level. This seems to show that the null hypothesis is not true, which means that the AOA fitness values for performance are statistically better. Lastly, it can be concluded that the AOA algorithm is better for both standard color images and pathology images in terms of the different performance parameters and takes less time to run.

6.3 Results over *t*-Entropy for Standard Color Images

For the standard color images, Fig. 10 shows the segmented results of Fig. 7a using *t*-entropy as an objective function across **4, 6, and 8 thresholds** using different PIOA (AOA, ASO, HGSO, EO, AOS, FDA and NRO). *t*-entropy is used as the objective function in the numerical comparison of various PIOAs for standard images with 4 and 8 thresholds in Table 10. Here standard deviation (σ_f), fitness function $(\bar{f})$, Computational time (sec), PSNR, FSIM and SSIM used as numerous parameters for performance evaluation of segmented image. With addition the

Fig. 8 Segmented results of PIOA using Tsallis entropy over 4, 6, and 8 thresholds for Fig. 7a
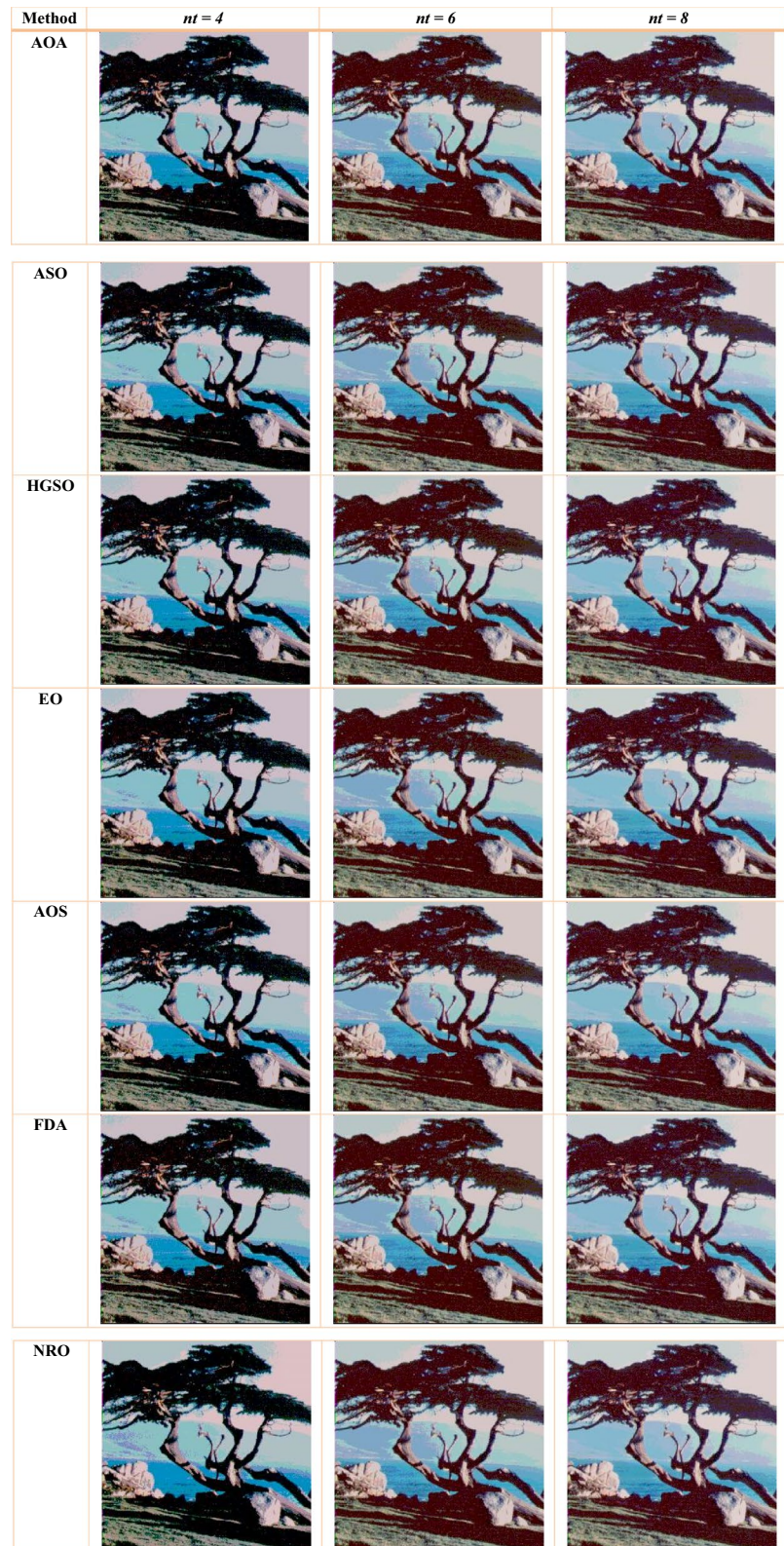
bold value in this table is represented the best performance value. Table 10 shows clearly that AOA gets the best results over the **threshold values of 4, 6 and 8** for all

parameters except for σ_f. In terms of characteristics such as PSNR and SSIM, NRO is the poorest of the studied PIOAs, but it has the best standard deviation $\left(\sigma_f\right)$ value. In

Table 6 Numerical comparison of PIOA for Tsallis Entropy as objective function over standard color image

Number of thresholds (nt)	PIOA	$\bar{f}$	σ_f	Time (s)	FSIM	PSNR	SSIM
4	AOA	**59,685.72**	**1.06E−08**	**2.3936**	**0.8974**	**16.86**	**0.6736**
	ASO	59,678.44	1.28E−05	2.4776	0.8971	16.48	0.6690
	HGSO	59,666.07	1.94E−08	2.4396	0.8968	16.36	0.6589
	EO	59,652.02	1.39E−07	2.4733	0.8961	16.32	0.6582
	AOS	59,539.12	1.34E−06	2.4983	0.8953	16.11	0.6531
	FDA	58,991.16	1.65E−08	2.6786	0.8911	15.91	0.6501
	NRO	58,863.94	1.76E−07	2.6998	0.8881	15.72	0.6409
6	AOA	**1,608,896.19**	**5.22E−07**	**3.3978**	**0.9339**	**21.41**	**0.8591**
	ASO	1,608,847.59	4.33E−06	3.4878	0.9334	21.32	0.8588
	HGSO	1,608,842.19	9.64E−07	3.4478	0.9333	21.30	0.8584
	EO	1,608,735.34	4.93E−05	3.4978	0.9325	21.11	0.8579
	AOS	1,608,642.75	3.87E−05	3.5977	0.9324	21.08	0.8571
	FDA	1,608,547.96	1.18E−06	3.6878	0.9320	21.01	0.8561
	NRO	1,608,524.24	5.59E−06	3.7954	0.9314	20.58	0.8540
8	AOA	**31,588,982.11**	**6.25E−06**	**4.3274**	**0.9544**	**23.79**	**0.8934**
	ASO	31,586,680.81	6.85E−06	4.4237	0.9540	23.78	0.8931
	HGSO	31,586,527.05	7.87E−06	4.4234	0.9539	23.66	0.8932
	EO	31,584,744.77	8.78E−05	4.4274	0.9531	23.61	0.8929
	AOS	31,573,136.42	4.59E−05	4.5279	0.9524	23.58	0.8927
	FDA	31,567,620.49	9.65E−06	4.6234	0.9519	23.48	0.8921
	NRO	31,563,879.07	9.99E−06	4.7908	0.9511	23.15	0.8914

Best results are highlighted in bold

Table 7 Comparison among PIOA depending on Wilcoxon p values over Standard Color image for Tsallis Entropy

Pair of PIOA	Tsallis Entropy over Standard Color Image					
	$nt=4$		$nt=6$		$nt=8$	
	p	h	p	h	p	h
AOA vs. AOS	<0.05	1	<0.05	1	<0.05	1
AOA vs. FDA	<0.05	1	<0.05	1	<0.05	1
AOA vs. EO	<0.05	1	<0.05	1	<0.05	1
AOA vs. HGSO	<0.05	1	<0.05	1	<0.05	1
AOA vs. ASO	<0.05	1	<0.05	1	<0.05	1
AOA vs. NRO	<0.05	1	<0.05	1	<0.05	1

addition, for a given threshold value, NRO requires the most computational time. On the other hand, **threshold value 8,** NRO imparts the worst result amongst all the tested PIOA's for the parameters namely computational time and FSIM whereas HGSO achieves the best standard deviation (σ_f) value. Consequently, for **threshold value 6**, AOA achieves the best results for all parameters considered, whereas FDA achieves the poorest results among all examined PIOAs for the parameters FSIM, PSNR, and SSIM. Additionally, for the same, NRO requires the most computational time. Table 11 displays the pair-wise

comparisons of PIOA (AOA vs. ASO; AOA vs. FDA; AOA vs. EO; AOA vs. HGSO; AOA vs. AOS; and AOA vs. NRO) based on Wilcoxon p-values for Standard Color images with t-entropy for **4, 6, and 8 thresholds**. The Wilcoxon p-values obtained and projected in Table 11 for threshold number 8 are less than 0.05 (5 percent significance level) with h = 1, which is an evident proof against the null hypothesis, implying that the AOA fitness values for performance are statistically superior. Nonetheless, this is not the case for threshold values 4 and 6, since the Wilcoxon p-values obtained are more than 0.05 (5 percent significant level) in a few instances, as seen in the table.

Fig. 9 Segmented results of
PIOA using Tsallis entropy over
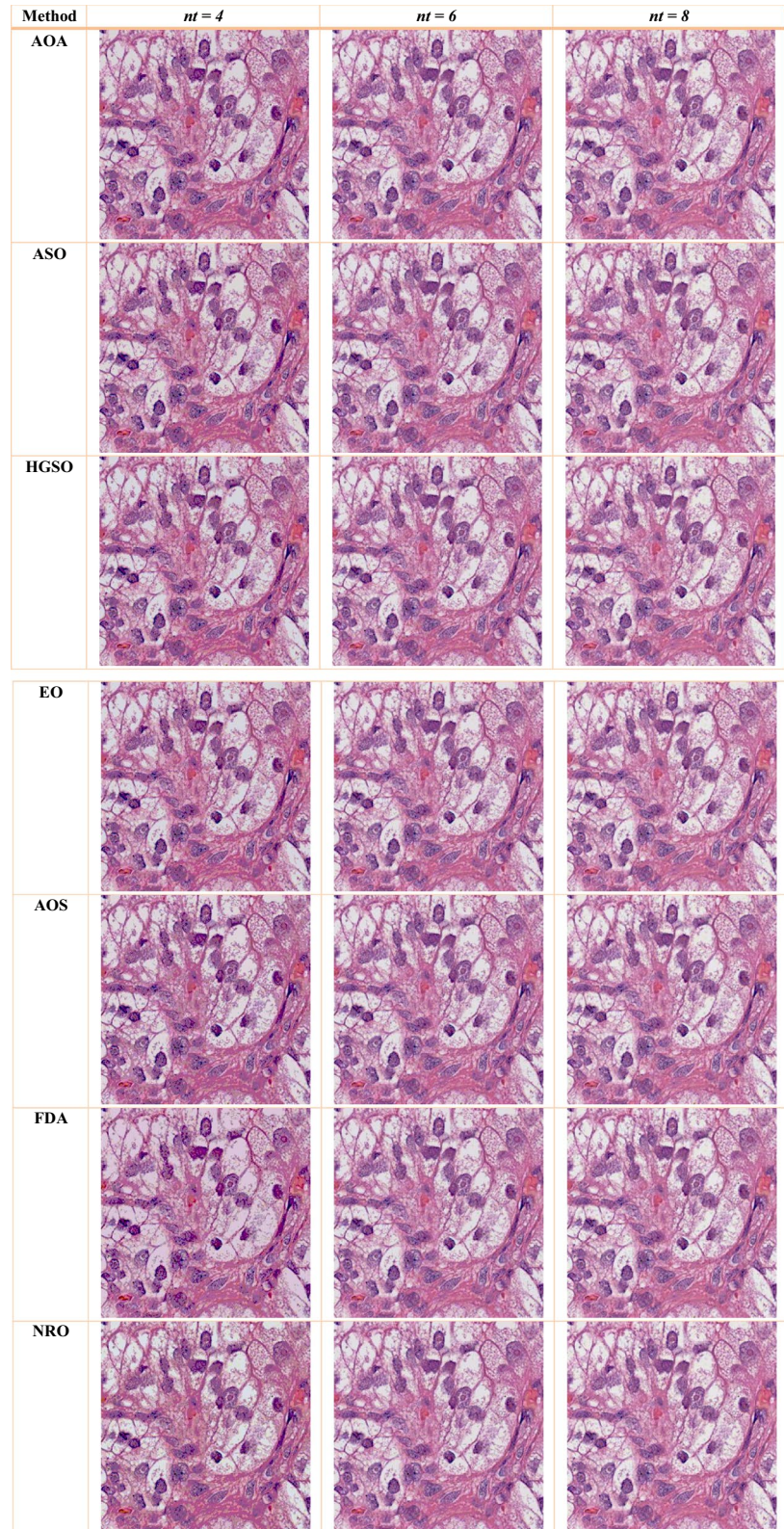4, 6, and 8 thresholds for Fig. 7b

Method	nt = 4	nt = 6	nt = 8
AOA			
ASO			
HGSO			
EO			
AOS			
FDA			
NRO			

Table 8 Numerical comparison of PIOA for Tsallis entropy as an objective function over Pathology Image

Number of thresholds (nt)	PIOA	$\bar{f}$	σ_f	Time (s)	FSIM	PSNR	SSIM
4	AOA	**48,954.63**	**2.42E−09**	**3.3815**	**0.9529**	**20.78**	**0.8756**
	ASO	48,723.18	3.01E−07	3.4848	0.9524	20.75	0.8756
	HGSO	48,582.67	3.24E−08	3.4381	0.9520	20.68	0.8751
	EO	48,399.59	3.01E−08	3.4795	0.9514	20.51	0.8711
	AOS	48,196.82	4.18E−07	3.5103	0.9511	20.48	0.8708
	FDA	47,971.37	5.29E−08	3.7320	0.9501	20.42	0.8702
	NRO	47,843.13	5.54E−08	3.7581	0.9498	20.29	0.8702
6	AOA	**1,330,965.12**	**3.54E−07**	**4.6167**	**0.9737**	**24.05**	**0.9319**
	ASO	1,330,950.62	9.29E−06	4.7274	0.9734	23.98	0.9315
	HGSO	1,330,938.83	6.20E−07	4.6782	0.9732	23.88	0.9311
	EO	1,330,929.24	7.69E−06	4.7397	0.9730	23.84	0.9309
	AOS	1,330,897.88	1.12E−06	4.8626	0.9724	23.81	0.9308
	FDA	1,330,781.67	1.44E−06	4.9735	0.9718	23.77	0.9301
	NRO	1,330,711.65	8.53E−06	5.1058	0.9714	23.76	0.9298
8	AOA	**24,692,789.31**	**5.10E−06**	**5.7602**	**0.9911**	**26.54**	**0.9578**
	ASO	24,680,419.73	5.41E−05	5.8787	0.9904	26.52	0.9575
	HGSO	24,671,330.66	3.95E−05	5.8783	0.9899	26.48	0.9574
	EO	24,670,834.45	1.57E−05	5.8832	0.9895	26.45	0.9571
	AOS	24,665,568.45	7.21E−05	6.0069	0.9887	26.39	0.9567
	FDA	24,663,457.67	7.07E−05	6.1243	0.9884	26.34	0.9561
	NRO	24,651,842.25	9.24E−05	6.2303	0.9882	26.28	0.9557

Best results are highlighted in bold

Table 9 Comparison among PIOA depending on Wilcoxon p values over Color Pathology Image for Tsallis Entropy

Pair of PIOA	Tsallis Entropy over Color Pathology Image					
	$nt=4$		$nt=6$		$nt=8$	
	p	h	p	h	p	h
AOA vs. AOS	<0.05	1	<0.05	1	<0.05	1
AOA vs. FDA	<0.05	1	<0.05	1	<0.05	1
AOA vs. EO	<0.05	1	<0.05	1	<0.05	1
AOA vs. HGSO	<0.05	1	<0.05	1	<0.05	1
AOA vs. ASO	<0.05	1	<0.05	1	<0.05	1
AOA vs. NRO	<0.05	1	<0.05	1	<0.05	1

6.4 Results over *t*-entropy for Pathology Images

Figure 11 illustrates the visual segmentation results of Fig. 7(b) utilizing several PIOA (AOA, ASO, HGSO, EO, AOS, FDA, and NRO) using t-entropy as the objective function across thresholds of 4, 6, and 8 for the Pathology picture. *t*-entropy is used as the objective function in the numerical comparison of various PIOAs for pathology images with 4 and 8 thresholds in Table 12. Here standard deviation $\left(\sigma_f\right)$, fitness function $\left(\bar{f}\right)$, Computational time (sec), PSNR, FSIM and SSIM used as numerous parameters for performance evaluation of segmented image. With addition the bold value

in this table is represented the best performance value. For every parameter considered, results in Table 12 clearly show that AOA achieves the greatest results over threshold values of 6. NRO, on the other hand, is the worst PIOA in terms of all criteria except for PSNR, whereas FDA is the worst in terms of PSNR. On the other hand for **threshold values 4 and 8,** AOA accomplishes the best result for every parameter taken into account except for that of the standard deviation $\left(\sigma_f\right)$. FDA and NRO achieves the best standard deviation $\left(\sigma_f\right)$ values for **threshold values 4 and 8** respectively. FDA performs worst for **threshold values 4 and 8** in terms of FSIM, PSNR and SSIM nonetheless; NRO consumes the most computation time. Table 13 tabulates the pair-wise

Fig. 10 Segmented results of PIOA using *t*-entropy over 4, 6, and 8 thresholds for Fig. 7a
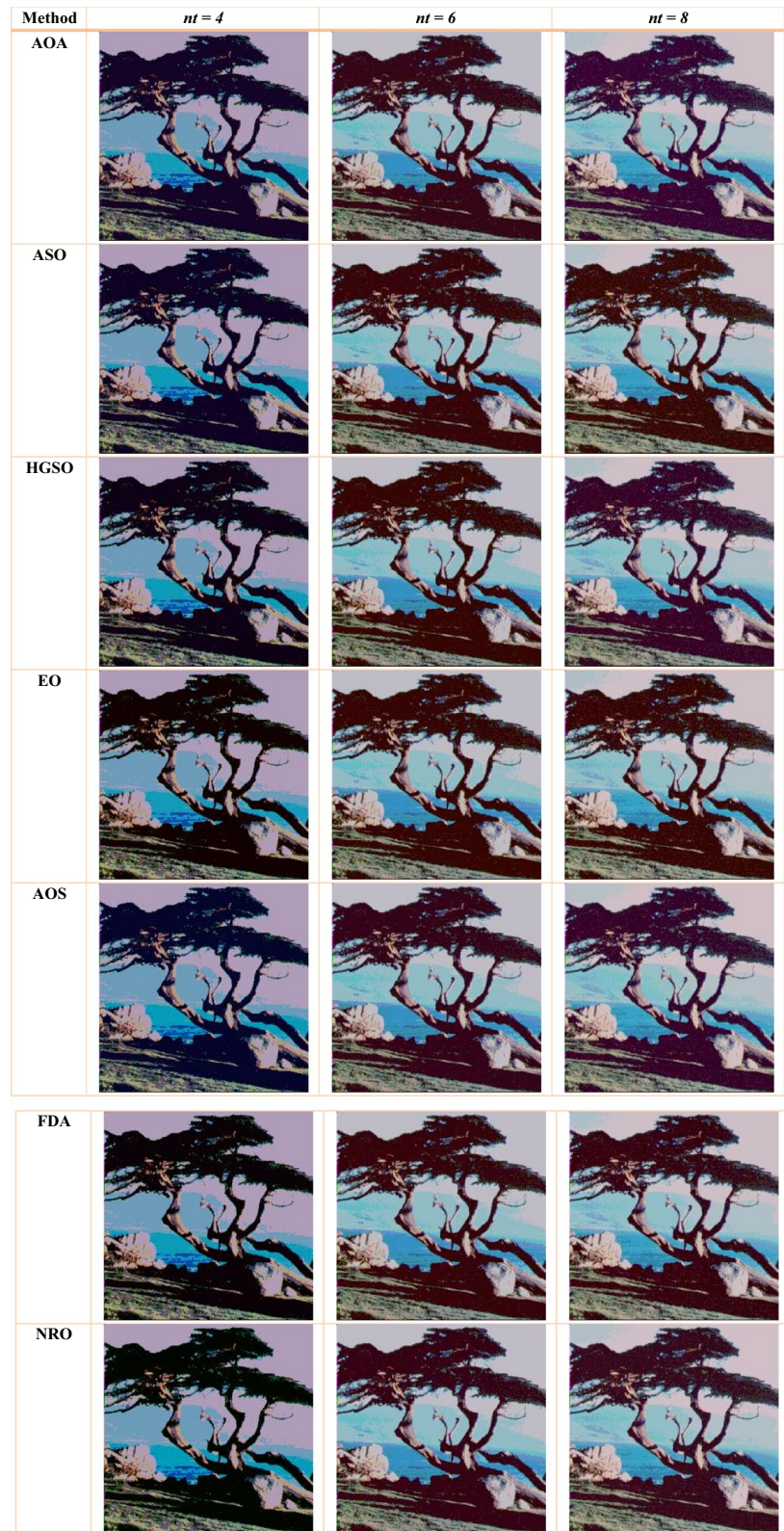
comparisons of PIOA (AOA vs. ASO; AOA vs. FDA; AOA vs. EO; AOA vs. HGSO; AOA vs. AOS; and AOA vs. NRO) based on Wilcoxon p-values for Standard Color images with t-entropy for **4, 6, and 8 thresholds**. The Wilcoxon p-values obtained and predicted in Table 13 for threshold number 8 are less than 0.05 (5 percent significance level) with h = 1,

Table 10 Numerical comparison of PIOA for *t*-entropy as an objective function over a standard color image

Number of thresholds (nt)	PIOA	$\bar{f}$	σ_f	Time (s)	FSIM	PSNR	SSIM
4	AOA	**0.585824**	1.21E−20	**4.0010**	**0.8422**	**15.35**	**0.7021**
	ASO	0.585823	2.02E−20	4.1414	0.8418	15.15	0.6998
	HGSO	0.585823	1.24E−20	4.0779	0.8413	15.12	0.6998
	EO	0.585823	1.09E−20	4.1343	0.8413	15.13	0.6995
	AOS	0.585823	1.67E−20	4.1760	0.8412	15.13	0.6992
	FDA	0.585822	**1.08E−20**	4.4774	0.8401	14.86	0.6899
	NRO	0.585822	1.34E−20	4.5129	0.8402	14.84	0.6895
6	AOA	**0.880116**	**1.23E−19**	**5.6796**	**0.9088**	**19.59**	**0.8271**
	ASO	0.880115	3.23E−18	5.8300	0.8989	19.52	0.8270
	HGSO	0.880115	4.17E−19	5.7632	0.8989	19.53	0.8268
	EO	0.880115	2.67E−19	5.8468	0.8988	19.48	0.8261
	AOS	0.880114	3.93E−19	6.0137	0.8985	19.49	0.8259
	FDA	0.880114	5.01E−19	6.1644	0.8981	19.46	0.8258
	NRO	0.880114	3.25E−19	6.3442	0.8978	19.45	0.8255
8	AOA	**1.126865**	1.77E−19	**7.2335**	**0.9289**	**21.98**	**0.8657**
	ASO	1.126851	1.64E−19	7.3945	0.9281	21.58	0.8622
	HGSO	1.126849	**1.39E−19**	7.3940	0.9279	21.53	0.8619
	EO	1.126846	5.47E−19	7.4006	0.9278	21.52	0.8619
	AOS	1.126834	2.51E−18	7.5686	0.9271	21.48	0.8611
	FDA	1.126817	2.46E−19	7.7283	0.9269	21.41	0.8608
	NRO	1.126799	3.58E−19	8.0081	0.9270	21.40	0.8604

Best results are highlighted in bold

Table 11 Comparison among PIOA depending on Wilcoxon *p* values over Standard Color image for *t*-entropy

| Pair of PIOA	*t*-Entropy over Standard Color Image					
	$nt = 4$		$nt = 6$		$nt = 8$	
	p	h	p	h	p	h
AOA vs. AOS	> 0.05	0	> 0.05	0	< 0.05	1
AOA vs. FDA	< 0.05	1	< 0.05	1	< 0.05	1
AOA vs. EO	> 0.05	0	> 0.05	0	< 0.05	1
AOA vs. HGSO	> 0.05	0	> 0.05	0	< 0.05	1
AOA vs. ASO	> 0.05	0	> 0.05	0	< 0.05	1
AOA vs. NRO	< 0.05	1	< 0.05	1	< 0.05	1

indicating that the AOA performance fitness values are statistically better. Nonetheless, this is not the case for **threshold values 4 and 6**, since the Wilcoxon p-values obtained are more than 0.05 (5 percent significant level) in a few instances, as seen in the table.

6.5 Discussion on the Performance Comparison Among Objective Functions

According to Table 6 and Table 10, it is clear that Tsallis and t-entropy, two famous objective functions for standard color pictures, outperform for every PIOA over characteristics such as fitness function $(\bar{f})$, standard deviation (σ_f), com-

putational time (sec), FSIM, and PSNR for all PIOAs. Tsallis entropy, on the other hand, surpasses t-entropy in terms of SSIM for nt = 6 and 8; nevertheless, for nt = 4, t-entropy yields superior results. When utilizing Tsallis entropy to segment standard color images, different PIOA's require almost half the computation time for different threshold values than using t-entropy as an objective function. It can be concluded and inferred from the experimental results that every PIOA combination with Tsallis entropy surpasses the PIOA combination with t-entropy in almost all circumstances and in almost all parameters. While this is true, the PIOA in combination with Tsallis entropy yields better results and is clearly superior as an objective function for any threshold

Fig. 11 Segmented results of PIOA using *t*-entropy over 4, 6, and 8 thresholds for Fig. 7b
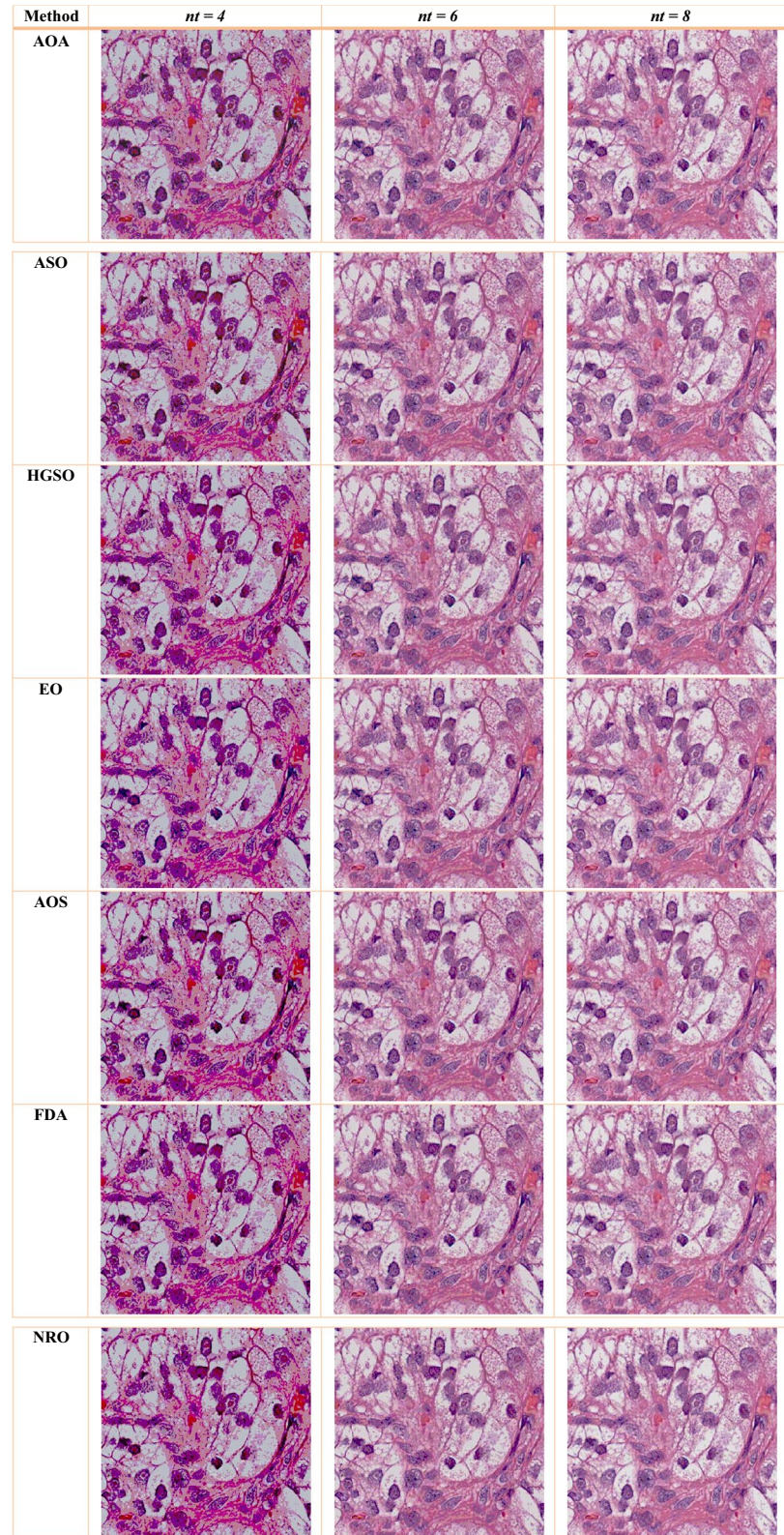
value, it is clear by looking at Tables 8 and 12, which show that this is also true for every parameter evaluated in the scenario. This demonstrates that, despite the fact that

t-entropy is a recently proposed notion that is rarely used in image segmentation, Tsallis entropy as an objective function gives an intriguing and unorthodox option for regular color

Table 12 Numerical comparison of PIOA for *t*-entropy as an objective function over Pathology Image

Number of thresholds (*nt*)	PIOA	$\bar{f}$	σ_f	Time (s)	FSIM	PSNR	SSIM
4	AOA	**0.572714**	2.63E−20	**4.4582**	**0.8851**	**15.35**	**0.7218**
	ASO	**0.572714**	8.35E−20	4.6146	0.8849	15.34	0.7217
	HGSO	**0.572714**	5.34E−20	4.5438	0.8850	15.31	0.7215
	EO	**0.572714**	2.06E−20	4.6067	0.8846	13.25	0.7214
	AOS	**0.572714**	3.16E−20	4.6531	0.8845	13.21	0.7213
	FDA	0.572713	**2.04E−20**	4.9890	0.8841	13.14	0.7211
	NRO	0.572713	6.53E−20	5.0285	0.8838	13.11	0.7208
6	AOA	**0.856319**	**2.32E−19**	**6.3285**	**0.9622**	**21.22**	**0.8876**
	ASO	0.856318	6.11E−18	6.4961	0.9621	21.22	0.8875
	HGSO	0.856318	5.89E−19	6.4217	0.9618	21.15	0.8873
	EO	0.856318	5.05E−19	6.5148	0.9615	21.12	0.8871
	AOS	0.856318	3.43E−19	6.7008	0.9614	21.11	0.8871
	FDA	0.856316	9.19E−19	6.8687	0.9611	21.08	0.8867
	NRO	0.856317	6.13E−19	7.0691	0.9608	21.10	0.8867
8	AOA	**1.102992**	4.34E−19	**8.0600**	**0.9851**	**24.42**	**0.9384**
	ASO	1.102982	3.13E−19	8.2394	0.9845	24.33	0.9381
	HGSO	1.102964	4.23E−19	8.2388	0.9842	24.32	0.9378
	EO	1.102959	1.06E−18	8.2462	0.9840	24.28	0.9377
	AOS	1.102957	6.56E−18	8.4334	0.9836	24.19	0.9375
	FDA	1.102949	4.65E−19	8.6113	0.9834	24.15	0.9371
	NRO	1.102941	**2.77E−19**	8.9231	0.9833	24.14	0.9368

Best results are highlighted in bold

Table 13 Comparison among PIOA depending on Wilcoxon *p* values over Color Pathology Image for *t*-entropy

Pair of PIOA	*t*-entropy over Color Pathology Image					
	nt = 4		*nt* = 6		*nt* = 8	
	p	*h*	*p*	*h*	*p*	*h*
AOA vs. AOS	> 0.05	0	> 0.05	0	< 0.05	1
AOA vs. FDA	< 0.05	1	< 0.05	1	< 0.05	1
AOA vs. EO	> 0.05	0	> 0.05	0	< 0.05	1
AOA vs. HGSO	> 0.05	0	> 0.05	0	< 0.05	1
AOA vs. ASO	> 0.05	0	> 0.05	0	< 0.05	1
AOA vs. NRO	< 0.05	1	< 0.05	1	< 0.05	1

image segmentation problems. Both Tsallis entropy and t-entropy as objective functions in association with various PIOA are more suited for pathology pictures than ordinary color images in general, according to this analysis. According to the tables described above, a further examination shows that the processing time rises, but the values for FSIM and PSNR and SSIM also increase as the number of thresholds grows for the objective function under consideration. For a typical color image and a pathologic image, Figs. 12 and 13 provide a visual comparison between Tsallis and t-entropy in terms of processing time, FSIM, PSNR, and SSIM. The average values of the computational time, FSIM, PSNR, and SSIM for the graphs have been computed by averaging the results of all the seven tested PIOA over all the tested standard color images and pathology images.

7 Conclusion

In this paper, the author conducted a depth review of AOA which is a recent physics-inspired optimization problem. Along with AOA the author also presents several optimization techniques inspired by the non-linear physics phenomena applied over standard color and pathology images for MLT image segmentation problems. In this study, the author considers two significant objective functions i.e. Tsallis and
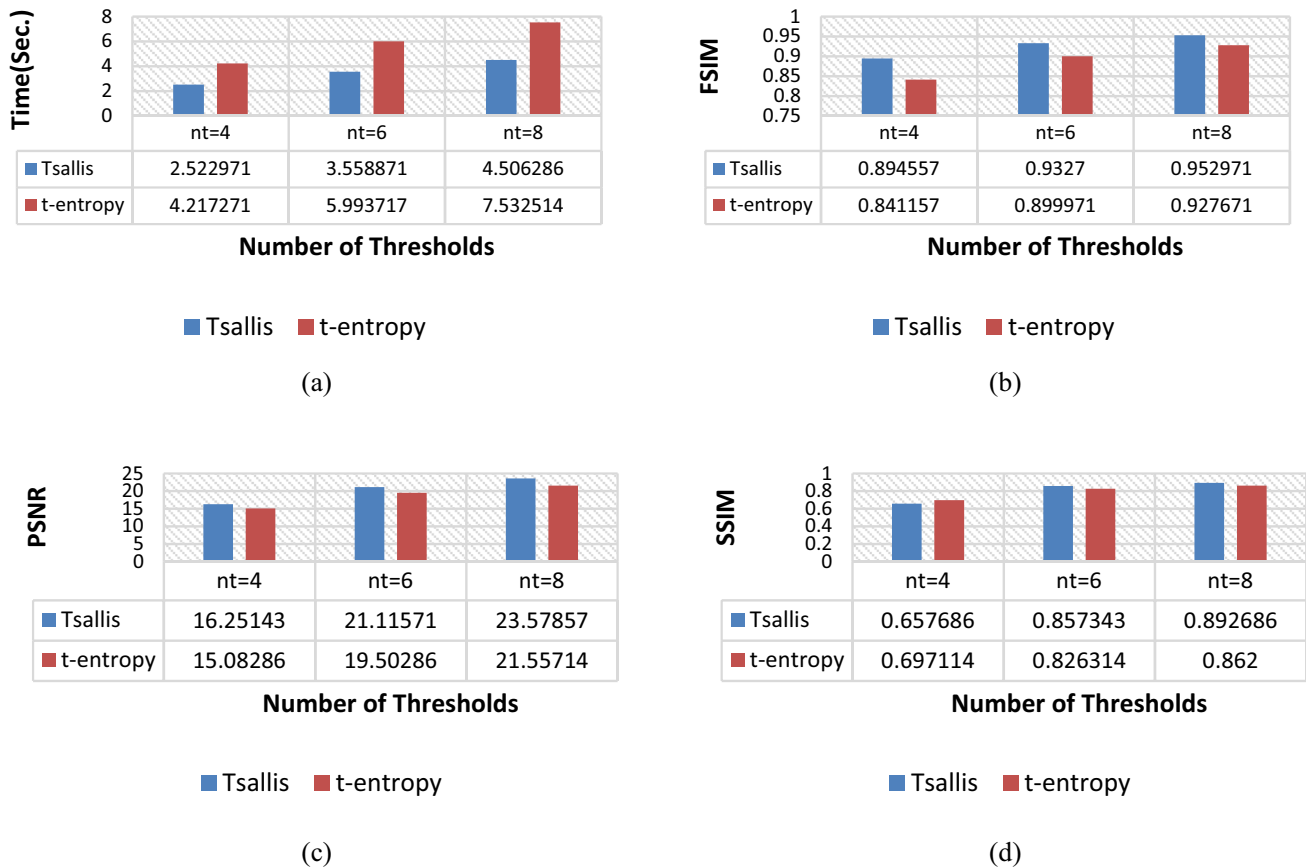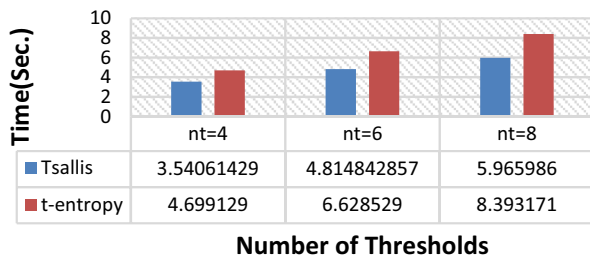
Time(Sec.)	nt=4	nt=6	nt=8
Tsallis	2.522971	3.558871	4.506286
t-entropy	4.217271	5.993717	7.532514

Number of Thresholds

■ Tsallis ■ t-entropy

(a)

FSIM	nt=4	nt=6	nt=8
Tsallis	0.894557	0.9327	0.952971
t-entropy	0.841157	0.899971	0.927671

Number of Thresholds

■ Tsallis ■ t-entropy

(b)

PSNR	nt=4	nt=6	nt=8
Tsallis	16.25143	21.11571	23.57857
t-entropy	15.08286	19.50286	21.55714

Number of Thresholds

■ Tsallis ■ t-entropy

(c)

SSIM	nt=4	nt=6	nt=8
Tsallis	0.657686	0.857343	0.892686
t-entropy	0.697114	0.826314	0.862

Number of Thresholds

■ Tsallis ■ t-entropy

(d)

Fig. 12 Comparison among Tsallis and *t*-entropy over Standard Color Images

t-entropy. An intense experiment has been carried out to demonstrate the significance of different PIOA in the field of MLT image segmentation and the comparison among the different methods namely AOA, ASO, HGSO, EO, AOS, FDA, and NRO has been carried forward to identify the appropriate one for the same. The performance of AOA along with several other PIOA are evaluated here with help of PSNR, FSIM, SSIM, standard deviation, fitness function, etc. Quite a few contributions have been projected in this paper as highlighted in the introduction section out of which, *t*-entropy for MLT predominantly with PIOA marks the key contribution. The results and core proclamation of this paper have been recapitulated as follows:

(a) It is evident from the numerical results that AOA has shown its competence and accuracy above other PIOA's signifying that AOA is the most suitable PIOA for the MLT image segmentation process of the standard color images as well as pathology images over the entire threshold's values (4, 6, and 8) for every parameter taken into account with Tsallis' entropy as objective function thus paving its way towards other realms of image processing with fastest execution time. On the
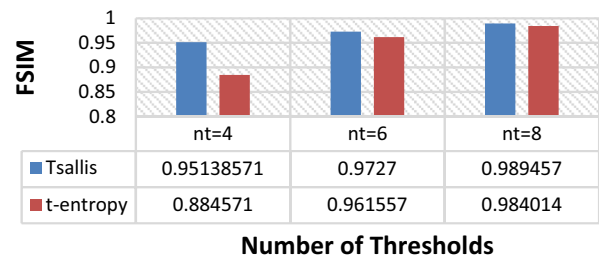
other hand, NRO for the same scenario displayed the worst result.

(b) Further, using *t*-entropy as the objective function, the experimental result generated showcased that for different performance parameters different PIOA has its own significance. Also, the performance of PIOA varied as per the different threshold values taken into account. However, from the overall analysis, it can be stated that AOA in most of the cases outperforms other PIOA's considered in this paper.

(c) In addition, every PIOA generates better results in terms of computational effort and quality parameters every time Tsallis' entropy as the objective function is taken into account for both variants of imagery in comparison to that of the *t-entropy* taken under similar circumstances.

(d) Each PIOA's considered in this paper and highlighted in Table 1, consumes almost half of the computation time for different threshold values considering Tsallis entropy to segment the standard color images as compared to segmentation using *t*-entropy as an objective function. However, in general, it can be stated that the computation time consumed by different PIOA using
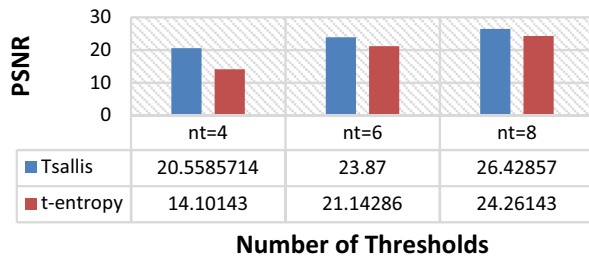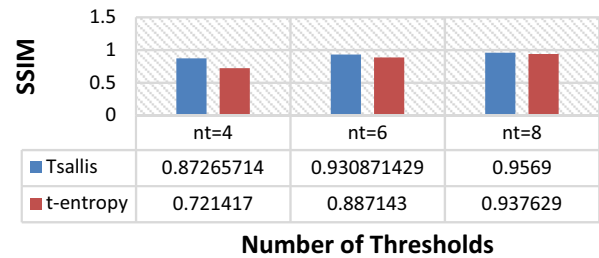
	nt=4	nt=6	nt=8
Tsallis	3.54061429	4.814842857	5.965986
t-entropy	4.699129	6.628529	8.393171

Number of Thresholds

Time(Sec.)

■ Tsallis   ■ t-entropy

(a)

	nt=4	nt=6	nt=8
Tsallis	0.95138571	0.9727	0.989457
t-entropy	0.884571	0.961557	0.984014

Number of Thresholds

FSIM

■ Tsallis   ■ t-entropy

(b)

	nt=4	nt=6	nt=8
Tsallis	20.5585714	23.87	26.42857
t-entropy	14.10143	21.14286	24.26143

Number of Thresholds

PSNR

■ Tsallis   ■ t-entropy

(c)

	nt=4	nt=6	nt=8
Tsallis	0.87265714	0.930871429	0.9569
t-entropy	0.721417	0.887143	0.937629

Number of Thresholds

SSIM

■ Tsallis   ■ t-entropy

(d)

Fig. 13 Comparison among Tsallis and *t*-entropy over Color Pathology Images

Tsallis entropy is much lesser than consumed using *t*-entropy.

(e) The experimental conclusion demonstrates that both objective functions studied in this research in relation to various PIOA are better suited for pathology images than the usual color image.

(f) Even though as mentioned earlier that *t*-entropy is the newly established concept rarely employed in image segmentation, Tsallis entropy as an objective function proves its way towards flattering the researcher by becoming an interesting and unconventional preference/choice for standard color image and pathology image segmentation tasks.

(g) As the number of thresholds rises, it is also shown that computation time increases, and PSNR and the other SSIM metrics do as well for both the objective function.

The experimental analysis unquestionably draws attention to the researcher to explore and examine AOA for MLT based image segmentation and broadly in the image processing domain [62]. This in turn leads to several research directions and challenges and the same has been brought to light below:

(a) Two-Dimensional (2D) objective functions [7] like 2D Cross, 2D-Renyi, 2D Tsallis, 2D Otsu, etc., could be considered and applied over diverse PIOA in the domain of image segmentation making it a challenging task.

(b) Other variants of images such as standard grayscale, satellite images, and other medical images such as MRI, CT, histology, etc., could be considered using the numerous PIOA experimented in this paper.

(c) In addition, an improved variant of *t*-entropy or 2D *t*-entropy needs to be initiated and further applied in the domain of image segmentation to yield an exceptional outcome.

(d) Last but not the least, initiating hybrid AOA or a hybrid PIOA to explore multi-objective MLT could be a striking work for the future (Table 14).

Table 14 Nomenclature

N	Population size	PID	Proportional-integral-derivative
O$_i$	*ith* object within the *N*	AVRs	Automatic voltage regulators
ub$_i$	Upper bound in the search space	FA-LS	Firefly algorithm-based least square
lb$_i$	Lower bounds in the search space	PSOPC-LS	passive congregation based least square
vol$_i$	Volume of *ith* object	ABC-LS	Artificial bee colony based least square
den$_i$	Density of *ith* object	AOA-LS	Archimedes optimization algorithm-based least square
acc$_i$	Acceleration (acc) of the *ith* object	AOADBN-MTP	Archimedes Optimization Algorithm with Deep Belief Network-based mobile network traffic prediction
TF	Transfer operator *TF* is used in AOA to convert search from exploration to exploitation	BSO	Bus splitting optimization
t_{max}	Maximum iteration	*FSIM*	Feature Similarity Index
t	Iteration number	*PSNR*	Peak Signal to Noise Ratio
d^{t+1}	Density in $t+1$ iteration	*SSIM*	Structural Similarity index
acc_i^{t+1}	Acceleration of *ith* object in $T+1$ iteration	PEMFC	Proton Exchange Membrane Fuel Cell
den_i^{t+1}	Density of *ith* object in $T+1$ iteration	SOFC	Solid Oxide Fuel Cell
vol_i^{t+1}	Volume of *ith* object in $T+1$ iteration	SSOA	Slap Swarm Optimization Algorithm
acc_{mr}	Acceleration of random material	ASO	Atom search Optimizer
den_{mr}	Density of random material	LAO	Levy Flight Archimedes optimizer
vol_{mr}	volume of random material	PSO	Particle swarm optimization
acc_{best}	Acceleration of best object	MAPE	Mean absolute percentage error
x_i^{t+1}	Position of *ith* object in $T+1$ iteration	SMES	Superconducting magnetic energy storage
F	Direction of motion	CHB	Cascaded H-bridge
I-AOA	Improve Archimedes Optimization Algorithm	MLI	Multilevel inverter
EAOA	Enhanced Archimedes Optimization Algorithm	SHE	Selective harmonic elimination
MAOA	Modified Archimedes Optimization Algorithm	RMSE	Root mean square error
DFOES	Decomposition–forecasting–optimization ensemble system	CFNN	Cascade-forward neural network
DG	Distributed Generation	DTDNN	Distributed time-delay neural network
MPPT	Maximum power point tracker	STSA-NN	Sine Tree-Seed Algorithm neural network
PEMFC	Proton exchange membrane fuel cell	AOA-NN	Archimedes Optimization Algorithm with Neural Network
SOPs	Soft open points	FFNN	feed-forward neural network
HC	Hosting capacity		
PV	Photovoltaic		

Declarations

Conflict of interest On behalf of all authors, the corresponding author states that there is no conflict of interest. The authors declare that they have no conflict of interest.

Research Involving Human and Animal Rights This article does not contain any studies with human participants or animals performed by any of the authors.

References

1. Pal NR, Pal SK (1993) A review on image segmentation techniques. Pattern Recogn 26(9):1277–1294
2. Dhal KG, Das A, Ray S, Sarkar K, Gálvez J (2021) An analytical review on rough set based image clustering. Arch Comput Methods Eng 1–30
3. Ray S, Das A, Dhal KG, Gálvez J, Naskar PK (2022) Whale optimizer-based clustering for breast histopathology image segmentation. Int J Swarm Intell Res 13(1):1–29
4. Dhal KG, Fister Jr I, Das A, Ray S, Das S (2018) Breast histopathology image clustering using cuckoo search algorithm. In:

Proceedings of the 5th student computer science research conference, pp 47–54

5. Dhal KG, Das A, Ray S, Gálvez J, Das S (2020) Nature-inspired optimization algorithms and their application in multi-thresholding image segmentation. Arch Comput Methods Eng 27(3):855–888

6. Dhal KG, Ray S, Das A, Das S (2019) A survey on nature-inspired optimization algorithms and their application in image enhancement domain. Arch Comput Methods Eng 26(5):1607–1638

7. Rai R, Das A, Dhal KG (2022) Nature-inspired optimization algorithms and their significance in multi-thresholding image segmentation: an inclusive review. Evol Syst. https://doi.org/10.1007/s12530-022-09425-5

8. Salcedo-Sanz S (2016) Modern meta-heuristics based on nonlinear physics processes: a review of models and design procedures. Phys Rep 655:1–70

9. Biswas A, Mishra KK, Tiwari S, Misra AK (2013) Physics-inspired optimization algorithms: a survey. J Optim. https://doi.org/10.1155/2013/438152

10. Hashim FA, Hussain K, Houssein EH, Mabrouk MS, Al-Atabany W (2021) Archimedes optimization algorithm: a new metaheuristic algorithm for solving optimization problems. Appl Intell 51(3):1531–1551

11. Azizi M (2021) Atomic orbital search: a novel metaheuristic algorithm. Appl Math Model 93:657–683

12. Karami H, Anaraki MV, Farzin S, Mirjalili S (2021) Flow Direction Algorithm (FDA): a novel optimization approach for solving optimization problems. Comput Ind Eng 156:107224

13. Faramarzi A, Heidarinejad M, Stephens B, Mirjalili S (2020) Equilibrium optimizer: a novel optimization algorithm. Knowl-Based Syst 191:105190

14. Hashim FA, Houssein EH, Mabrouk MS, Al-Atabany W, Mirjalili S (2019) Henry gas solubility optimization: a novel physics-based algorithm. Futur Gener Comput Syst 101:646–667

15. Zhao W, Wang L, Zhang Z (2019) Atom search optimization and its application to solve a hydrogeologic parameter estimation problem. Knowl-Based Syst 163:283–304

16. Wei Z, Huang C, Wang X, Han T, Li Y (2019) Nuclear reaction optimization: a novel and powerful physics-based algorithm for global optimization. IEEE Access 7:66084–66109

17. Chakraborty S, Paul D, Das S (2021) t-Entropy: a new measure of uncertainty with some applications. arXiv preprint arXiv:2105.00316

18. Houssein EH, Helmy BED, Rezk H, Nassef AM (2021) An enhanced Archimedes optimization algorithm based on Local escaping operator and Orthogonal learning for PEM fuel cell parameter identification. Eng Appl Artif Intell 103:104309

19. Desuky AS, Hussain S, Kausar S, Islam MA, El Bakrawy LM (2021) EAOA: an enhanced Archimedes optimization algorithm for feature selection in classification. IEEE Access 9:120795–120814

20. Akdag O (2022) A improved Archimedes optimization algorithm for multi/single-objective optimal power flow. Electric Power Syst Res 206:107796

21. Yao B, Hayati H (2021) Model parameters estimation of a proton exchange membrane fuel cell using improved version of Archimedes optimization algorithm. Energy Rep 7:5700–5709

22. Cheng M, Qin T, Yang J (2022) Node localization algorithm based on modified Archimedes optimization algorithm in wireless sensor networks. J Sens

23. Sun X, Wang G, Xu L, Yuan H, Yousefi N (2021) Optimal estimation of the PEM fuel cells applying deep belief network optimized by improved Archimedes optimization algorithm. Energy 237:121532

24. Singh R, Kaur R (2022) A novel Archimedes optimization algorithm with levy flight for designing microstrip patch antenna. Arab J Sci Eng 47(3):3683–3706

25. Chen J, He Q, Li SY (2022) Archimedes optimization algorithm based on golden Levy guidance mechanism. J Comput Appl

26. Zhang L, Wang J, Niu X, Liu Z (2021) Ensemble wind speed forecasting with multi-objective Archimedes optimization algorithm and sub-model selection. Appl Energy 301:117449

27. Ali ZM, Diaaeldin IM, El-Rafei A, Hasanien HM, Aleem SHA, Abdelaziz AY (2021) A novel distributed generation planning algorithm via graphically-based network reconfiguration and soft open points placement using Archimedes optimization algorithm. Ain Shams Eng J 12(2):1923–1941

28. Li Y, Zhu H, Wang D, Wang K, Kong W, Wu X (2021) Comprehensive optimization of distributed generation considering network reconstruction based on Archimedes optimization algorithm. In: IOP conference series: earth and environmental science, vol 647, no 1). IOP Publishing, p 012031

29. Fathy A, Alharbi AG, Alshammari S, Hasanien HM (2022) Archimedes optimization algorithm based maximum power point tracker for wind energy generation system. Ain Shams Eng J 13(2):101548

30. Yousri D, Shaker Y, Mirjalili S, Allam D (2022) An efficient photovoltaic modeling using an Adaptive Fractional-order Archimedes optimization algorithm: validation with partial shading conditions. Sol Energy 236:26–50

31. Aribowo W, Muslim S, Suprianto B, Haryudo S, Hermawan AC (2021) Intelligent control of power system stabilizer based on Archimedes optimization algorithm-feed forward neural network. Int J Intell Eng Syst 14(3):43–53

32. Wang J, Zhan C, Li S, Zhao Q, Liu J, Xie Z (2022) Adaptive variational mode decomposition based on Archimedes optimization algorithm and its application to bearing fault diagnosis. Measurement 191:110798

33. Fathy A, Babu TS, Abdelkareem MA, Rezk H, Yousri D (2022) Recent approach based heterogeneous comprehensive learning Archimedes optimization algorithm for identifying the optimal parameters of different fuel cells. Energy 248:123587

34. Chen L, Rezaei T (2021) A new optimal diagnosis system for coronavirus (COVID-19) diagnosis based on Archimedes optimization algorithm on chest X-ray images. Comput Intell Neurosci

35. Neggaz I, Fizazi H (2022) An intelligent handcrafted feature selection using Archimedes optimization algorithm for facial analysis. Soft Comput 1–30

36. Eid A, El-Kishky H (2021) Multi-objective Archimedes optimization algorithm for optimal allocation of renewable energy sources in distribution networks. In: International conference on digital technologies and applications. Springer, Cham, pp 65–75

37. Anand S (2021) Archimedes optimization algorithm: Heart disease prediction: Archimedes optimization algorithm: heart disease prediction. Multimed Res 4(3)

38. Annrose J, Rufus N, Rex CR, Immanuel DG (2022) A cloud-based platform for soybean plant disease classification using Archimedes optimization based hybrid deep learning model. Wirel Pers Commun 122(4):2995–3017

39. Abdelbadie HT, Taha AT, Hasanien HM, Turky RA, Muyeen SM (2022) Stability enhancement of wind energy conversion systems based on optimal superconducting magnetic energy storage systems using the Archimedes optimization algorithm. Processes 10(2):366

40. Khan RA, Farooqui SA, Sarwar MI, Ahmad S, Tariq M, Sarwar A, Shah Noor Mohamed A (2021) Archimedes optimization algorithm based selective harmonic elimination in a cascaded H-bridge multilevel inverter. Sustainability 14(1):310

41. Janamala V, Radha Rani K (2022) Optimal allocation of solar photovoltaic distributed generation in electrical distribution networks using Archimedes optimization algorithm. Clean Energy 6(2):271–287

42. Annrose J, Rufus NHA, Rex CES, Immanuel DG (2021) Soybean plant disease classification using Archimedes optimization algorithm based hybrid deep learning model

43. Liang G, Panahi F, Ahmed AN, Ehteram M, Band SS, Elshafie A (2021) Predicting municipal solid waste using a coupled artificial neural network with Archimedes optimisation algorithm and socioeconomic components. J Clean Prod 315:128039

44. Agwa A, Elsayed S, Ahmed M (2022) Design of optimal controllers for automatic voltage regulation using Archimedes optimizer. Intell Autom Soft Comput 31(2):799–815

45. Apon HJ, Abid MS, Morshed KA, Nishat MM, Faisal F (2021) Power system harmonics estimation using hybrid Archimedes optimization algorithm-based least square method. In: 2021 13th international conference on information & communication technology and system (ICTS), pp 312–317. IEEE

46. Zaki MA, Mahmoud T, Atia M, Osman ESAEA (2021) Optimal sizing and sitting of electric vehicle charging station by using Archimedes optimization algorithm technique. Int J Power Electron Drive Syst 12(4):2557–2569

47. Selvamanju E, Shalini VB (2022) Archimedes optimization algorithm with deep belief network based mobile network traffic prediction for 5G cellular networks. In: 2022 4th international conference on smart systems and inventive technology (ICSSIT), pp 370–376. IEEE

48. Doğan E, Yörükeren N. Enhancement of transmission system security with Archimedes optimization algorithm

49. Hannon HAA, Latif HK, Abdulsadda AT (2022) Archimedes optimization algorithm based fractional MPPT for enhancing performance and efficiency of photovoltaic systems. Optoelectron Laser 41(4):225–240

50. Dinkar SK, Deep K, Mirjalili S, Thapliyal S (2021) Opposition-based laplacian equilibrium optimizer with application in image segmentation using multilevel thresholding. Expert Syst Appl 174:114766

51. bdel-Basset M, Chang V, Mohamed R (2020) A novel equilibrium optimization algorithm for multi-thresholding image segmentation problems. Neural Comput Appl 1–34

52. Qi H, Zhang G, Jia H, Xing Z (2021) A hybrid equilibrium optimizer algorithm for multi-level image segmentation. Math Biosci Eng 18(4):4648–4678

53. Kurban R, Durmus A, Karakose E (2021) A comparison of novel metaheuristic algorithms on color aerial image multilevel thresholding. Eng Appl Artif Intell 105:104410. https://doi.org/10.1016/j.engappai.2021.104410

54. Ray S, Parai S, Das A, Dhal KG, Naskar PK (2022) Cuckoo search with differential evolution mutation and Masi entropy for multilevel image segmentation. Multimed Tools Appl 81(3):4073–4117

55. Ray S, Das A, Dhal KG, Gálvez J, Naskar PK (2021) Cauchy with whale optimizer based eagle strategy for multi-level color hematology image segmentation. Neural Comput Appl 33(11):5917–5949

56. Hinojosa S, Dhal KG, Abd Elaziz M, Oliva D, Cuevas E (2018) Entropy-based imagery segmentation for breast histology using the stochastic fractal search. Neurocomputing 321:201–215

57. Anitha J, Pandian SIA, Agnes SA (2021) An efficient multilevel color image thresholding based on modified whale optimization algorithm. Expert Syst Appl 178:115003

58. Dhal KG, Das A, Ray S, Gálvez J (2021) Randomly attracted rough Firefly algorithm for histogram based fuzzy image clustering. Knowl-Based Syst 216:106814. https://doi.org/10.1016/j.knosys.2021.106814

59. Jegou H, Douze M, Schmid C (2008) Hamming embedding and weak geometric consistency for large scale image search. In: European conference on computer vision. Springer, Berlin, pp 304–317. https://lear.inrialpes.fr/~jegou/data.php

60. Irshad H, Montaser-Kouhsari L, Waltz G, Bucur O, Nowak JA, Dong F, Beck AH (2014) Crowdsourcing image annotation for nucleus detection and segmentation in computational pathology: evaluating experts, automated methods, and the crowd. In: Pacific symposium on biocomputing Co-chairs, pp 294–305. https://tcgadata.nci.nih.gov/tcga/

61. García S, Molina D, Lozano M, Herrera F (2009) A study on the use of non-parametric tests for analyzing the evolutionary algorithms' behaviour: a case study on the CEC'2005 special session on real parameter optimization. J Heuristics 15(6):617–644

62. Dhal KG, Das A, Gálvez J, Ray S, Das S (2020) An overview on nature-inspired optimization algorithms and their possible application in image processing domain. Pattern Recognit Image Anal 30(4):614–631